4.4   ABSTRACT

The experimental study presented in this Paper is aimed at evaluating (1) the hydraulic performance of a needle-punched GCL using both standard liquids (i.e. de-ionized water) and organic compounds (i.e. diesel oil) in order to estimate the change in hydraulic conductivity and swelling ability upon contact or permeation with hydrocarbons; (2) the hydraulic conductivity of GCL samples saturated at different initial gravimetric water contents with the aim to investigate the effect of initial water saturation on hydrocarbon containment performances; (3) the swelling and hydraulic performances of an innovative material obtained by mixing sodium bentonite with a polymer.

4.5   INTRODUCTION

Geosynthetic Clay Liners (GCLs) are the most popular manufactured clay barriers used in pollution containment applications. GCLs generally contain a thin layer of sodium bentonite (dry thickness between 4 and 10 mm), sandwiched between two geotextiles or glued to a geomembrane, that ensures excellent containment performances regarding both advective and, if coupled with an attenuation layer, diffusive contaminant transport, when permeated with standard liquids (i.e. de-ionized water, DW).

Especially in the specific applications of landfill covers and bottom barriers, the use of GCLs is now well established. However, in the last decade, new GCL applications, requiring their use for hydrocarbon containment, have found growing interest. In this particular area, the main GCL application is the secondary containment aimed at preventing subsoil dispersion of accidental oil spills through primary lining system (HDPE) from hydrocarbon storage tanks (underground or on surface).

As hydrocarbon containment is concerned, a reduction of the barrier efficiency (with respect to the hydraulic conductivity values commonly measured with DW) can be expected due to the reactive nature of sodium bentonite. In fact petroleum products,

which are characterized by dielectric constant values significantly lower than the dielectric constant of water, produce a compression of the diffusive double layer (DDL) of bentonite particles and consequently a decrease of the hydraulic containment performances of the barrier.

Although today there are few practical examples of use of these technologies for the hydrocarbon containment, a field trial aimed at containing hydrocarbons using a composite liner (geomembrane + GCL) was illustrated by Li et al. (2002). Moreover, not only recently, but also in the past, some laboratory studies were carried out to investigate the hydraulic performance of clayey soil permeated with organic solutions (Brown et al., 1984; Fernandez and Quigley, 1985; Foreman and Daniel, 1986; Daniel et al., 1993; Boldt-Lepping et al., 1996; Shan and Lai, 2002; Yang and Lo, 2004; Rowe et al., 2004; Rowe et al., 2005).

The experimental study presented in this Paper is aimed at evaluating (1) the hydraulic performance of a needle-punched GCL using both standard liquids (i.e. de-ionized water) and organic compounds (i.e. diesel oil) in order to estimate the change in hydraulic conductivity and swelling ability upon contact or permeation with hydrocarbons; (2) the hydraulic conductivity of GCL samples saturated at different initial gravimetric water contents with the aim to investigate the effect of initial water saturation on hydrocarbon containment performances; (3) the swelling and hydraulic performances of an innovative material obtained by mixing sodium bentonite with a polymer in contact with water and hydrocarbons fluids.

In particular, the polymer selection has been individualised in accordance with the following selection criteria: (1) maintenance of dispersed bentonite structure, preventing DDL contraction and cracking (2) resistance to permeant solution washout, (3) resistance to biological degradation, (4) affinity to organic compounds and (5) production efficiency and sustainability.

4.6   MATERIALS AND METHODS

4.6.1   Bentonites

4.6.1.1 Geosynthetic Clay Liner and natural sodium bentonite

The GCL used in this study is reinforced (needle-punched) and contains powdered natural sodium bentonite, encapsulated between a non-woven polypropylene geotextile and a woven polypropylene geotextile. The GCL is characterized by a dry thickness of 6 mm and a bentonite mass per unit area equal to 5000 kg/m^2 (at 12% average moisture content).

Powder bentonite, which is contained inside the GCL, is characterized by a cation exchange capacity (CEC, measured using methylene blue adsorption method) equal to 105 meq/100g.

In Figure 4.9 the natural sodium bentonite particle size distribution related to the GCL is reported.
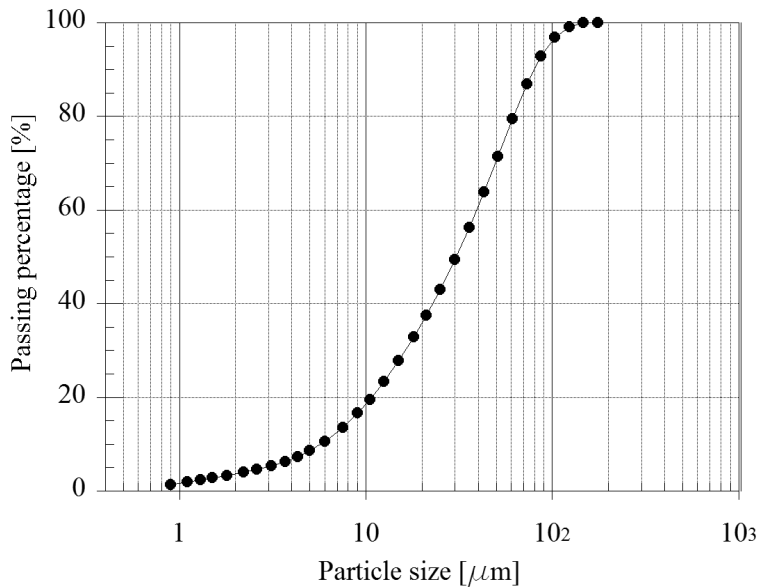

Figure 4.9 - Particle size distribution of powdered NaB contained in the GCL.

The mineralogical composition, evaluated through the x-ray diffraction analysis shown in Figure 4.10, gives a bentonite mainly composed by smectite determinated by calcite, quartz, mica and gypsum quantification.

4.6.1.2 Modified bentonites

The polymer modified bentonites used in this study mainly consist of natural sodium bentonite manufactured by adding different percentage of the VISCOGEL®-B4 (montmorillonite reacted with quaternary ammonium organic compounds) produced by Laviosa. In order to obtain modified bentonites, materials were separately dried at 60°C and then mixed at the dry state.
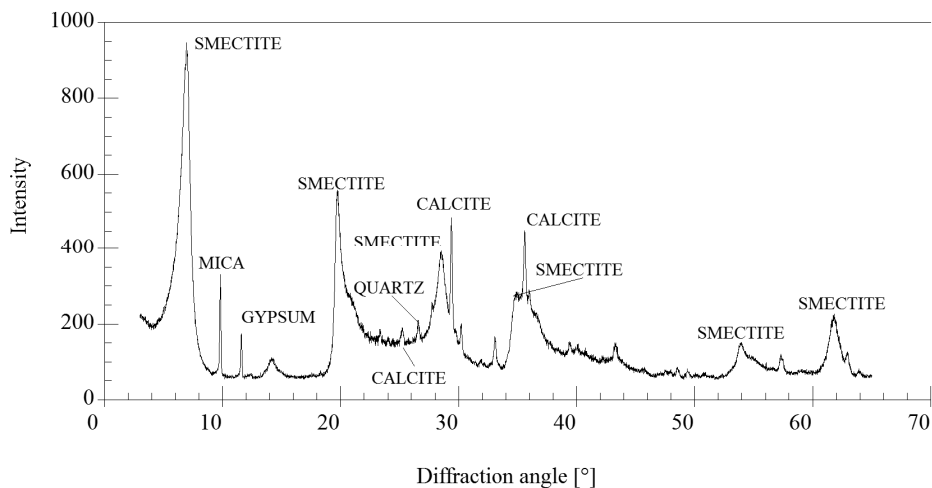

Figure 4.10 - XRD mineralogical composition of powdered NaB contained in the studied GCL.

4.6.2 Permeant liquids

The tests were performed using de-ionized water as 'standard permeant liquid' and diesel oil as hydrocarbon reference because of its massive commercial deployment.

Diesel oil is a product of the primary distillation of petroleum and it presents a distillation range between 160° C and 380° C. At room temperature diesel oil is liquid and it has a boiling point between 180° and 360° C. Moreover it presents the following properties: viscosity equal to 0.002 Pa·s and density equal to 850 kg/m^3.

4.6.3   Testing methods and equipments

4.6.3.1 Free swell test

The tests performed in the laboratory activity using natural and modified bentonites in contact with DW and diesel oil were performed with reference to ASTM 5890 test method. According to this standard, 2.00 ± 0.01 g of dried clay are dusted in each cylinder containing the liquid. After 16 h of undisturbed standing, the volume level of the top of settled bentonite was recorded as the swell index (SI [mL/2g]).

Free swell test can estimate the volume change of bentonite after hydration (Katsumi et al., 2008) and can give qualitative measurement of osmotic swelling and hydraulic performance of bentonites subjected to different standard (i.e. DW) or non-standard (i.e. diesel oil) solutions.

4.6.3.2 Hydraulic conductivity test

Departing from the qualitative nature of the test above, hydraulic conductivity test allows for the quantitative evaluation of barrier performances. The GCL and modified bentonite were tested accordingly to ASTM D 5887-99 and ASTM D 5084, using flexible wall permeameters and the "falling head method".

GCL specimens were prepared following the procedure described by ASTM D 5887-99 and successively they were saturated with DW at different initial water content. The initial water content was controlled before starting the test, measuring the total amount of DW adsorbed by the specimen inside the permeameter.

Powder specimens were prepared using the following procedure: powder mixture was loosely deposited at dry state in a steel mold inside the permeameter. The bulk dry density was approximately equal to the gravimetric one (0.79 g/cm^3 for VISCOGEL$^®$ B4- bentonite mixture at 30% content by weight of VISCOGEL$^®$ B4) in order to simulate the initial conditions of the bentonite in a GCL. Inside the mold the flexible membrane was adhered to the specimen, so that, after removing the mold, the permeameter could be completely assembled. The specimen was saturated with diesel oil for approximately 12 h and then permeated.

All specimens had 101.6 mm diameter and initial height equal to 6 mm and 10 mm for GCL and the powdered specimen respectively. Tests were performed using a

maximum hydraulic gradient of 500 (the hydraulic gradient is calculated as the hydraulic head difference across the specimen divided by the specimen length).

4.7   RESULTS

4.7.1   Free swell tests

Figure 4.11 shows the results of the tests performed with diesel oil on the natural bentonite-VISCOGEL[®]B4 mixtures characterized by different polymer content, ranging from 10% to 90% content by weight of VISCOGEL[®]B4. Moreover the SI of pure natural bentonite (i.e. 0%) and pure VISCOGEL[®]B4 (i.e. 100%) are plotted.
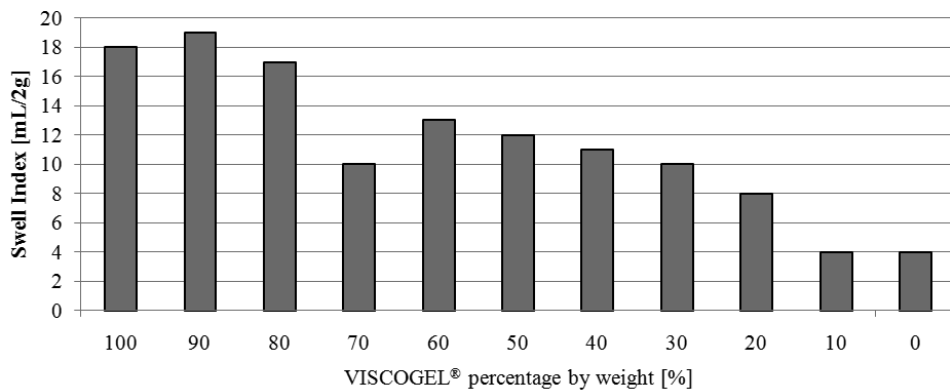

Figure 4.11 - Swell index of powdered natural and modified bentonite samples in contact with diesel oil.

For an easier identification of the effect of the degradation caused by hydrocarbons on swelling performance of the natural and modified material, it should be noted that the result of the same test, conducted on the natural bentonite in contact with DW, identified a turbid sample. This kind of samples does not show a precise interface between the settled bentonite and the upper clear liquid. In these cases, bentonite forms a stable suspension and it is not possible to determinate an accurate SI, therefore a conventional value equal to 100 mL/2g has been assigned.

The swelling ability of the mixtures increases by increasing VISCOGEL®B4 content by weight. In particular, the percentage by weight equal to 30% has been considered for further evaluation due its double SI if compared to the pure bentonite value.

4.7.2 Hydraulic conductivity tests

The hydraulic conductivity tests were carried out on GCL specimens saturated with DW at different initial gravimetric water contents and subsequently permeated with diesel oil.

A test with standard liquid was also performed by both hydrating and permeating the GCL with DW aimed to compare the results obtained with hydrocarbons permeability.

In order to compare the results of these tests, a parameter that quantifies the permeability of the material regardless to the permeating fluid has to be used. This parameter is the coefficient of permeability, k, related to the hydraulic conductivity, K, through the following equation:

$$k = \frac{K_f \cdot \mu_f}{\rho_f \cdot g}$$

[4.13]

Where: k is the permeability coefficient, which is a function of material intrinsic characteristics, K_f is the hydraulic conductivity coefficient referred to the permeant fluid, μ_f is the viscosity coefficient of the permeant fluid, ρ_f is the density of the permeant fluid and g is the gravitational acceleration.

The tests were performed in a flexible-wall permeameter under an initial effective confining stress of 27.5 kPa (calculated as the difference between the water pressure applied in the cell and the specimen backpressure) and with a maximum hydraulic gradient equal to 500.

Results are plotted in Figure 4.12 in terms of GCL permeability coefficient as functions of pore volumes of flow, which is a dimensionless parameter that represents the elapsed time of permeation, calculated as accumulated outflow divided by the pore volume of the specimen. Results in terms of hydraulic conductivity referred to the permeant fluid are also reported in the graph.
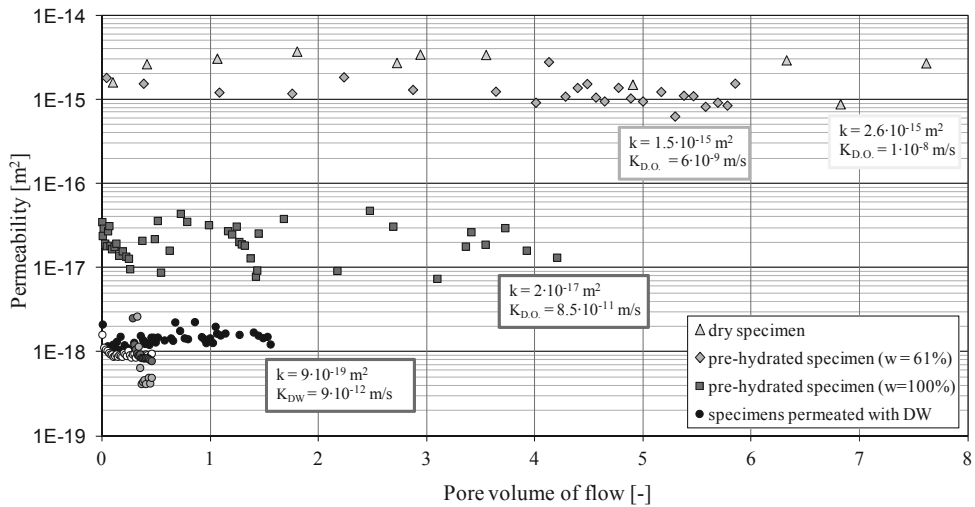
Figure 4.12 - Permeability of GCL specimens to diesel oil (D.O.) starting from different initial water content compared with the permeability of a GCL specimen to DW.

The results plotted in Figure 4.4 show that GCL permeability coefficient with respect to diesel oil decreases as initial water content increases. In particular, during the permeation of the dry GCL with diesel oil a very high value of permeability coefficient, equal to $k = 2.6 \cdot 10^{-15}$ m2 (more than 3 order of magnitude higher than the value obtained with DW), was measured. Such a decrease of bentonite hydraulic performance must necessarily be explained by a change in both the soil microscopic structure, due to a contraction of DDL of bentonite particles, and the soil macroscopic structure, due to clay shrinkage and the formation of cracks and macropores, that behave as preferential pathways for hydraulic flow and determine a strong increase in hydraulic conductivity.

In Figure 4.13 the permeability results with diesel oil are compared with those obtained by Rowe et al. (2005) for a partially hydrated GCL permeated with jet fuel at 20°C. The data are plotted as a function of the initial gravimetric water content of GCL specimens.

When the results obtained on specimens pre-hydrated with DW before permeation with diesel oil, reported both in Figure 4.5 (as a function of the initial gravimetric water content) and in Figure 4.4 (as a function of the pore volume of flow) are analyzed, it is clear that, for initial gravimetric water contents equal or lower than

61%, the bentonite contained in the GCL cracks and is characterized by a very low hydraulic performance, similar to that obtained with the dry GCL specimen, on the other hand, for water contents equal or higher than 100%, the bentonite undergoes only the effect of DDL contraction at the microscopic scale that has less influence on hydraulic performance. Therefore the permeability value measured during permeation of the GCL specimen pre-hydrated at 100% initial water content, equal to k = 2·10^{-17} m2, results only little more than 1 order of magnitude higher than the value obtained with DW.
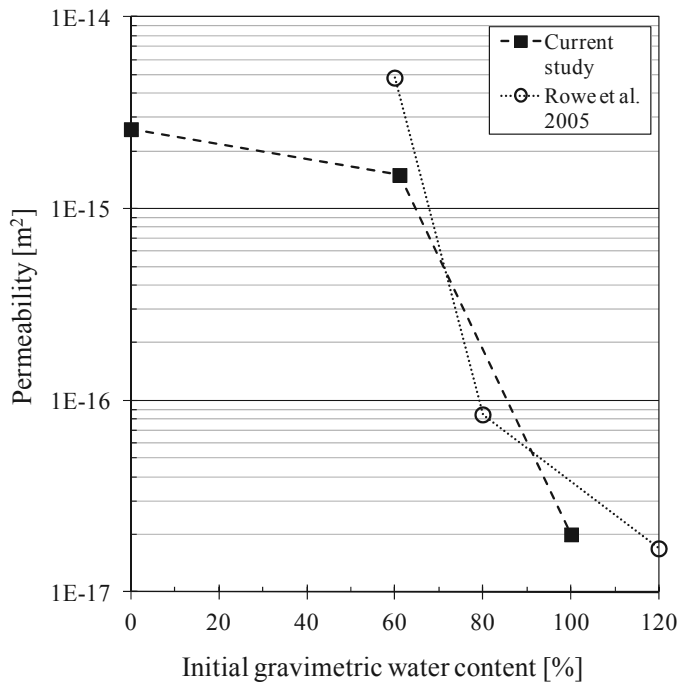

Figure 4.13 Permeability of GCL specimens to diesel oil (D.O.) against initial gravimetric water content compared with the results obtained by Rowe et al. (2005) using jet fuel.

Figure 4.13 shows that the trend obtained in this study is perfectly comparable with the results obtained by Rowe et al. (2005).

In order to evaluate the improvement in hydraulic performances induced by polymers, an hydraulic conductivity test was performed on the VISCOGEL®B4 - bentonite mixture containing a percentage by weigh of VISCOGEL®B4 equal to

30%. A dry modified specimen was permeated and obtained results are plotted in Figure 4.14.
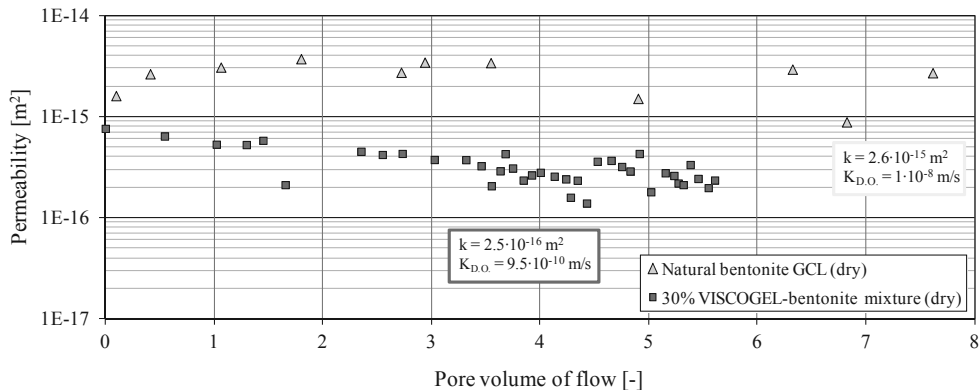

Figure 4.14 - Permeability of 30%VISCOGEL-bentonite mixture to diesel oil compared with the results obtained with the standard dry GCL.

The results obtained in terms of permeability of the dry modified bentonite are compared in Figure 4.14 with those obtained with the dry natural bentonite GCL. The permeability of the modified specimen results equal to k = 2.5·10^{-16} m^2 which is approximately one order of magnitude lower than the value obtained for the dry GCL.

4.8   CONCLUSIONS

The results of this study show that the permeability of the partially pre-hydrated GCL tested with diesel oil decreases as the initial gravimetric water content increases, in accordance with the previous studies (Rowe et al., 2005).

In particular, when the confining stress is 27.5 kPa, GCL specimen pre-hydrated at initial water content equal or higher than 100% performs considerably better than those characterized by lower initial water content values. This result can be explained assuming that the strong decrease of bentonite hydraulic performance measured by permeating samples characterized by an initial water content lower than 100% is due to the formation of cracks and macropores, that behave as preferential pathways for hydraulic flow and determine the remarkable increase in

hydraulic conductivity. On the contrary, the specimens characterized by higher initial water content, only the soil microstructure changes, due to the contraction of DDL of bentonite particles. This last phenomenon determines an increase in the effective porosity (i.e. available for the permeation), causing a lower increase in hydraulic conductivity.

The swelling tests performed on the bentonite specimens modified by the addition of increasing percentages of VISCOGEL[®]B4 show an increment of the mixture swelling ability increasing the polymer percentage.

The permeation of the modified bentonite (30% VISCOGEL[®]B4 content by weight) with diesel oil confirmed the qualitative results obtained by the swelling tests. The permeability coefficient of the modified bentonite at 27.5 kPa confining stress results about one order of magnitude lower than the value measured testing the dry GCL.

On the basis of the obtained experimental results, it is possible to state that the initial water content strongly affects the permeability of GCL. Although the pre-hydrated GCL seems to have a better behaviour in laboratory tests, it should be remarked that in situ conditions the GCL pre-hydration after installation could not easy reach a water content higher or equal to 100%. Moreover also the evaluation of the initial water content in situ could be very difficult or impossible.

However it can be inferred from the experimental results that an initial water content lower than 60% is sufficient to make the pre-hydration phase useless. As a result, the advantage of using bentonite - VISCOGEL[®]B4 mixture consists of the permeability independence from the initial water content.

ACKNOWLEDGEMENTS

REFERENCES

Belanteur, N., Tacherifet, S. & Pakzad, M. (1997). Étude des comportements mécanique, themo-mécanique et hydro-mécanique des argiles gonflantes et non gonflantes fortement compactées. Revue Française de Géotechnique **78**, 31-50.

Blatz, J. A., Graham, J., 2000. A system for controlled suction in triaxial tests. Geotechnique, **50**(4), 465-469.

Boldt-Leppin, B. E. J., Moir, D. H. & Headley, J. V. (1996). Use of organophilic clay in sand-bentonite as a barrier to diesel fuel. Canadian Geotechnical Journal, **33**(5), 705–719.

Bowders, J.J., Daniel, D.E., 1987. Hydraulic conductivity of compacted clay to dilute organic chemicals. Journal of Geotechnical Engineering, ASCE **113** (12), 1432-1448.

Broderick, G., Daniel, D., 1990. Stabilizing compacted clay against chemical attack. Journal of Geotechnical Engineering, ASCE, Reston, VA **116** (10), 1549 - 1566.

Brown, K. W., Thomas, J. C. & Green, J.W. (1984). Permeability of compacted soils to solvents, mixtures, and petroleum products. Land Disposal of Hazardous Waste, Proceedings, of the Tenth Annual Research Symposium, EPA-600/9–84–07. Municipal Environmental Research Laboratory, US Environmental Protection Agency, Cincinnati, OH, pp. 124–137.

Charbeneau, R. (2007). LNAPL distribution and recovery. API Pubblication 4760 (**1**). Available online on American Petroleum Institute website: http://www.api.org/environment-health-and-safety/clean-water/ground-water/lnapl/ldrm-form.aspx.

Cuisinier, O., Masrouri, F., 2002. Study of the hydromechanical behaviour of a swelling soil under high suctions. In proceedings 6th International workshop key issue in waste isolation research, Paris, **2**, 61-70.

Daniel, D. E., Shan, H. -Y. & Anderson, J. D. (1993). Effects of partial wetting on the performance of the bentonite component of a geosynthetic clay liner. Proceedings of Geosynthetics '93, Vancouver, Canada, pp. 1483–1496.

Fernandez, F., Quigley, R. M., (1988). Viscosity and dielectric constant controls on the hydraulic conductivity of clayey soil permeated with water-soluble organics. Canadian Geotechnical Journal **25**, 582 - 589.

Fernandez, F., Quigley, R. M. (1985). Hydraulic conductivity of natural clays permeated with simple liquid hydrocarbons. Canadian Geotechnical Journal, **22**(2), 205–214.

Foreman, D. E. & Daniel, D. E. (1986). Permeation of compacted clay with organic chemicals. Journal of Geotechnical Engineering, **112**(7), 669–681.

Mitchell, J.K., 1993. Fundamentals of Soil Behavior, 2nd Edition, John Wiley & Sons, Inc., New York, 437 p.

Mitchell, J.K., Madsen, F.T., 1987. Chemical effects on clay hydraulic conductivity. In: Woods, R.D. (Ed.), Geotechnical Practice for Waste Disposal ' 87. ASCE, pp. 87 116.

Rowe, R. K., Mukunoki, T., Li, M. H. & Bathurst, R. J. (2004). Effect of freeze-thaw on the permeation of Arctic diesel through a GCL. Journal of ASTM International, **1**(2), 1–13.

Rowe, R. K., Hurst, P. & Mukunoki, T. (2005). Permeating partially hydrated GCLs with jet fuel at temperatures from -20°C and 20°C. Geosynthetics International, **12**(6), 333-343.

Shackelford, C.D., 1994. Waste-soil interactions that alter hydraulic conductivity. In: Daniel, D.E., Trautwein, S.J. (Eds.), Hydraulic Conductivity and Waste Contaminant Transport in Soil, ASTM STP 1142. ASTM, West Conshohocken, PA, pp. 111 - 168.

Shackelford, C., D., Benson, C., H., Katsumi, T., Edil, T., B., Lin, L., 2000. Evaluation the hydraulic conductivity of GCLs permeated with non-standard liquids.

Yang, X. & Lo, I. M. C. (2004). Flow of gasoline through composite liners. Journal of Environmental Engineering, ASCE, **130**(8), 866–890.

Van Genuchten, M., Th. (1980). A closed-form equation for predicting the hydraulic conductivity of unsaturated soil. Soil Science Society of America Journal, **44**(5), 892-898.

Van Impe P. O. (2002). Consolidation, contaminant transport and chemico-osmotic effects in liner materials. PhD Dissertation, Ancona University, Ancona, Italy.

Villar, M.V. 1999. Inverstigation of the behaviour of bentonite by means of suction-controlled oedometer tests. Engineering Geology, **54**: 67-73.

Containment performances of a bentonite-based barrier constituted of municipal solid waste bottom ashes

REUSE OF MSWI BOTTOM ASH MIXED WITH NATURAL SODIUM BENTONITE AS LANDFILL COVER MATERIAL

by

Sara Puma*, Franco Marchese**, Andrea Dominijanni*, Mario Manassero*.

Affiliation:

*Department of Structural, Construction and Geotechnical Engineering. Politecnico di Torino, Corso Duca degli Abruzzi 24, 10129 Torino, Italy.

**Department of Environment, Land and Infrastructure. Politecnico di Torino, Corso Duca degli Abruzzi 24, 10129 Torino, Italy.

Corresponding author:

Sara Puma

Politecnico di Torino, Corso Duca degli Abruzzi 24, 10129 Torino, Italy.

sara.puma@polito.it

5.1 ABSTRACT

The research described in this study had the aim of evaluating the reuse of incinerator slag, mixed with sodium bentonite, for landfill capping system components. A characterization was performed on pure bottom ash (BA) samples from an incinerator in the North of Italy. The results show that the BA samples have appropriate properties as covers. The compacted dry unit weight of studied BA (16.2 kN/m^3) is lower than the average value that characterizes most conventional fill materials and this can be considered advantageous for landfill cover systems, since the fill has to be placed on low bearing capacity ground or where long-term settlement is possible. Moreover, direct shear tests show a friction angle of 43°, corresponding to excellent mechanical characteristics that can be considered an advantage against failure.

The hydraulic conductivity tests indicated a steady-state value of $8 \cdot 10^{-10}$ m/s for a mixture characterized by a bentonite content by weight of 10% which was a factor 10 better than required by Italian legislation on landfill covers. The results from a swell index test indicated that fine bentonite swells, even when divalent cations are released by the BA. The leaching behaviour of the mixture did not show any contamination issues and was far better than obtained for the pure BA. Thus, the BA-bentonite mixture qualifies as a suitable material for landfill cover in Italy. Moreover, owing to the low release of toxic compounds, the proposed cover system does not affect the leachate quality in the landfill.

5.2 KEYWORDS

Bentonite,
Hydraulic conductivity,
Incinerator bottom ash,
Landfill cover,
Leaching tests,
Shear strength.

5.3   INTRODUCTION

Municipal solid waste (MSW) management is one of the most relevant environmental problems of industrialized countries.

In 2010, for example, the production of MSW in Italy was estimated to be about 531 kg pro capita per year. The most common ways of treating non-recyclable solid waste, which constitutes about 426 kg pro capita per year, are landfilling (60%) and incineration (18%) (Eurostat, 2012). In spite of the reduction in waste volume that can be obtained from incineration, this process produces a non-negligible amount of slag, including 'bottom ash' (BA), or the material remaining on the combustor grid, and 'fly ash' (FA), or the component of ash carried by the air. Since the landfilling of these products represents a considerable contribution to the overall cost of incineration, interest in the reuse and recycling of incineration slag has increased significantly over the last decade. Several studies on BA have indicated the feasibility of its reuse as pre-treated or non pre-treated material in civil works (Mangialardi, 2001; Izquierdo et al., 2002; Appendino et al., 2004; Forteza et al., 2004; Birgisdottir et al., 2006; Plescia et al., 2006, Xue et al. 2008) or in glass production processes (Boccaccini et al., 1997; Wang et al., 1998; Sakai and Hiraoka, 2000; Romero et al., 2001; Wang et al., 2002; Monteiro et al., 2008).

The research described in this study was aimed at evaluating the reuse of incinerator slag, instead of the soil commonly used in soil-bentonite mixtures, for landfill capping purposes.

In Italy, the soils commonly used in capping systems (i.e. clays) are often not available close to the landfill site and this leads to supply costs. On the other hands, large quantities of BA from municipal solid waste incineration (MSWI BA), with mechanical properties that are appropriate for the construction of covers, are increasingly becoming available, due to the spread of incineration plants.

A BA from an incinerator in the North of Italy was selected for evaluation as a mixture with sodium bentonite. The chemical, physical, hydraulic and mechanical characterisation of the raw BA showed that the selected MSWI BA had appropriate chemical, physical and mechanical properties for covers, but did not have a suitable

hydraulic conductivity for Italian law requirements concerning the minimisation of rain water infiltration, i.e. hydraulic conductivity, K, $\leq 10^{-8}$ m/s guaranteed for a layer at least 0.5-m thick. For this reason, there was a need to create a mixture with less permeable material to satisfy the regulation. Many applications involving the use of sand-bentonite mixtures for hydraulic containment applications, where natural clayey soils are not readily or economically available, have been reported in literature (e.g. Abichou at al., 2002a; Abichou at al., 2002b; Alston et al., 1997; Castelbaum and Shackelford, 2009; Chapuis et al., 1992; Ebina et al., 2004; Garlanger et al., 1987; Gipson, 1985; Gleason et al., 1997; Haug and Wong, 1992; Haug and Bolt-Leppin, 1994; Howell and Shackelford, 1997; Kaoser et al., 2006, Kenney et al., 1992; Lundgren, 1981; O'Sadnick at al., 1995; Mollins et al., 1996; Sällfors and Öberg-Högsta, 2002; Stern and Shackelford, 1998; Teachavorasinskun and Visethrattana, 2006).

Since MSWI BA generally has a similar particle size distribution to that of a sand, or at least to that of a sand-fine gravel mixture (Monteiro et al. 2008; Dominijanni et al., 2009; Xue et al. 2009), the possibility of mixing BA with a natural material that would be able to achieve a relatively low hydraulic conductivity, such as natural sodium bentonite, was considered. The aim of the research was to verify whether the high swelling potential of sodium bentonite, in the presence of water, could produce a relatively tight, low hydraulic conductivity soil matrix for compacted BA-bentonite mixtures, as typically is the case of compacted sand-bentonite layers (Stern and Shackelford, 1998).

Like to the results obtained in other studies on fly ash (Creek and Shackelford, 1992; Shackelford and Glade, 1994; Kamon et al., 2000), the addition of bentonite and cement should decrease contaminant release from the BA, due to the adsorption of metals on the bentonite particles and the high level of cement alkalinity. Nevertheless, BAs generally have higher pHs than FAs and this higher alkalinity should limit the release of heavy metals, even without the addition of cement.

Chemical characterization, as well as batch and column leaching tests on the compacted BA and BA-bentonite mixture were performed to assess the pollutant release and, consequently, the environmental impact of the proposed cover system.

As far as the latter issue is concerned, the use of incinerator slag in capping systems does not, in principle, result in any additional risk of release of contaminants. In fact, if the material is reused in or below the hydraulic barrier of the capping system, the pollutants will be released inside the landfill and will produce the same environmental impact they would produce if landfilled. In this way, the slag, which is a secondary construction material, is reused with the result that landfilling costs are eliminated and supply costs are reduced, without any increase in environmental impact.

5.4   MATERIALS AND METHODS

The material constituents used in the laboratory evaluation were MSWI BA and a natural sodium bentonite. The physical and mechanical behaviour of the MSWI BA was characterized, and the results are briefly summarized in this section. The material was conserved in sealed containers until testing in order to prevent the loss of moisture due to evaporation. The plant that supplied the BA consists of a mobile grate and air cooled incineration line, which includes the lay-out, furnace capacity and process conditions reported in Table 5.1.

Table 5.1 – Primary features of the incineration line.

Feature	units	**BAs**
Project throughput	$kg\ h^{-1}$	1500
Grate length	m	5.5
Surface of grate	m^2	9
Mean furnace temperature	°C	~1150
Outlet bottom ash flow rate	$kg\ h^{-1}$	330
Outlet bottom ash temperature	°C	~860
Quenching tank volume	m^3	10.6
Mean quenching tank bottom ash residence time	s	570
Quenching water volume-bottom ash flow rate ratio	$L\ h\ kg^{-1}$	32.1

According to the particle-size distribution shown in Fig. 5.1, the sample had a median grain size, d_{50}, of 2.8 mm and a fines content of 0.11%, and was classified as a well-graded sand-fine gravel mixture (GW-SW) according to the Unified Soil Classification System (ASTM D 2487-00).
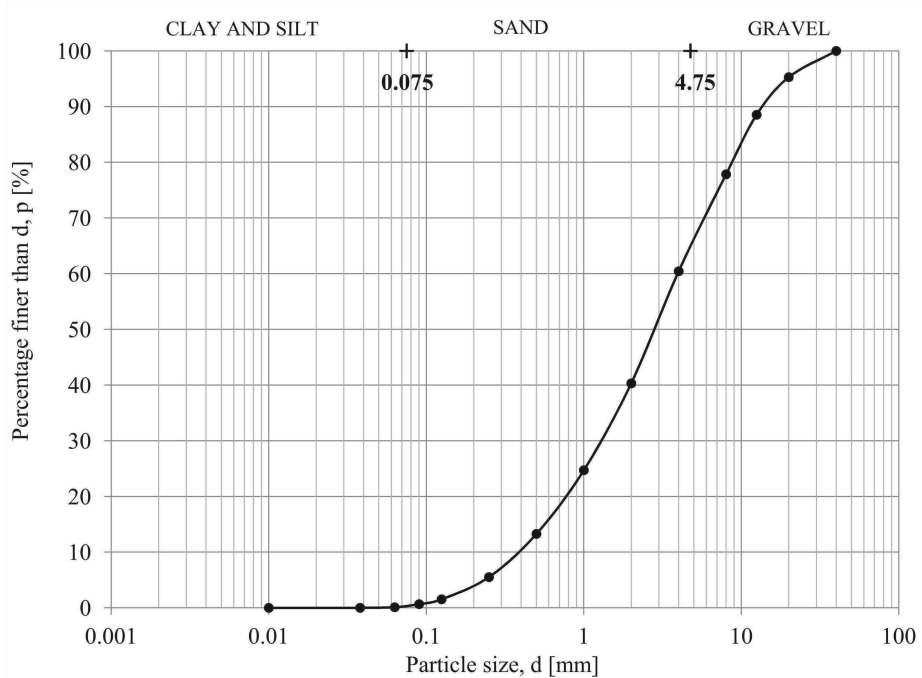

Figure 5.1 – Particle-size distribution of the bottom ash (dried procedure, ASTM D422 – 63).

Considering the possibility of reusing the BA as secondary construction material for landfill capping systems, the particle-size distribution suggested the possibility of dividing the raw material into two fractions: material finer than approximately 10 mm, corresponding to 70-80% by weight of the total amount of material, which would be suitable for a hydraulic barrier upon mixing with sodium bentonite, and coarser material which could be selected for a biogas collection layer or, in the absence of other possibilities, landfilled.

The results of tests for Atterberg limits, determined on the BA (particle diameter < 425 μm; ASTM D4318 – 00), showed a liquid limit of 42%, but no plastic limit.

Goh and Tay (1993) and Forteza et al. (2004) found the same non-plastic behaviour for MSWI fly ash and common ash.

The compaction characteristics of BA (particle diameter < 9.5 mm), determined using the standard Proctor procedure (ASTM D 698 – 00a), are presented in Fig. 5.2 in terms of dry unit weight versus water content; the zero air void curve was calculated using a specific gravity, G_S, of 2.53 (Poran and Ahtchi-Ali,1989; Monteiro et al., 2008).
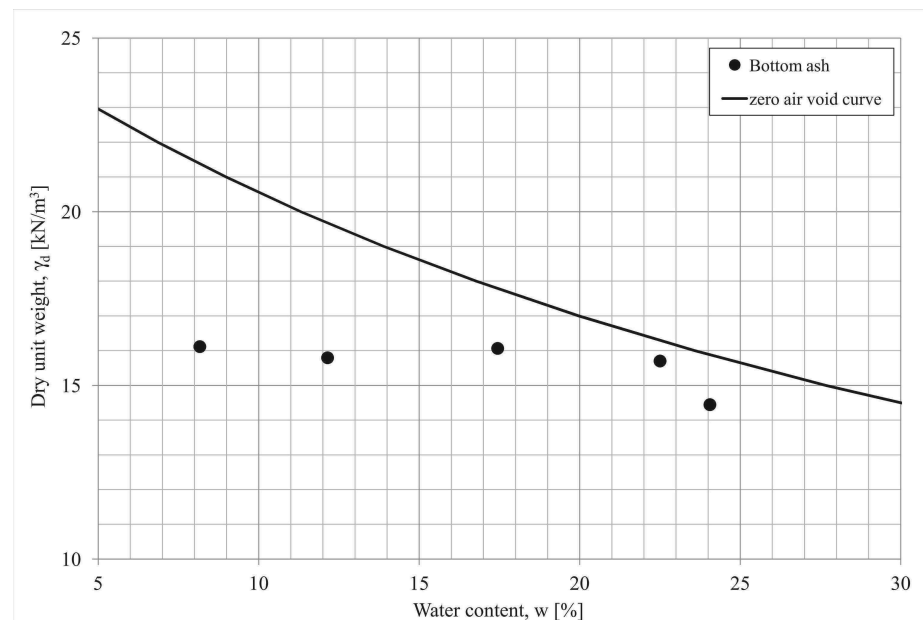

Figure 5.2 - Compaction curve of the bottom ash (ASTM D698).

According to the results of Proctor test, the BA does not behave like a fine grained soil, because its dry unit weight does not show an appreciable dependence on the water content. An average dry unit weight of 15.6 kN/m^3 was obtained, a value that is consistent with other reported results (Rogbeck and Hartlen, 1996; Wiles, 1996; Chandler et al., 1997; Izquierdo et al., 2001; Muhammad and Ashmawy, 2003; Forteza et al., 2004; Amaya and Amaya, 2007). This average dry unit weight for the BA is within the 13 to 18 kN/m^3 range for sand and the 14 to 21 kN/m^3 range for gravel reported by Lancellotta (2009), but is close to the lower limit. The fact that the compacted dry unit weight of the BA is generally lower than the average value

that characterizes most conventional fill materials can be considered advantageous, if the fill has to be placed on low bearing capacity ground or where long-term settlement is possible, such as in landfill cover systems (Okoli and Balafoutas, 1999).

The hydraulic conductivity, K, of the BA sample (particle diameter < 9.5 mm), measured in a fixed-wall permeameter (ASTM D 5856 – 95), was $K = 3 \cdot 10^{-7}$ m/s. This result is within the range of K values of $10^{-6} - 10^{-8}$ m/s reported for BA by others (Chandler et al., 1997; Wiles, 1996; Okoli and Balafoutas, 1999; Muhammad and Ashmawy, 2003).

Figure 3 – Ratio of shear to applied vertical stress as a function of the horizontal displacement for various normal stresses (50, 100, 200 kPa) in direct shear tests for the bottom ash (ASTM D3080-98).

The results of direct shear tests, performed on a dry material sample (particle diameter < 2.8 mm), are presented in Fig. 5.3 in terms of relative shear stress versus horizontal displacement, and in Fig. 5.4 in terms of the shear strain versus vertical strain, with specific reference to the peak, critical state and residual conditions.

Figure 4 – Variation in shear stress of the bottom ash in the peak, critical and residual conditions as a function of the applied vertical stress during direct shear tests (ASTM D3080-98).

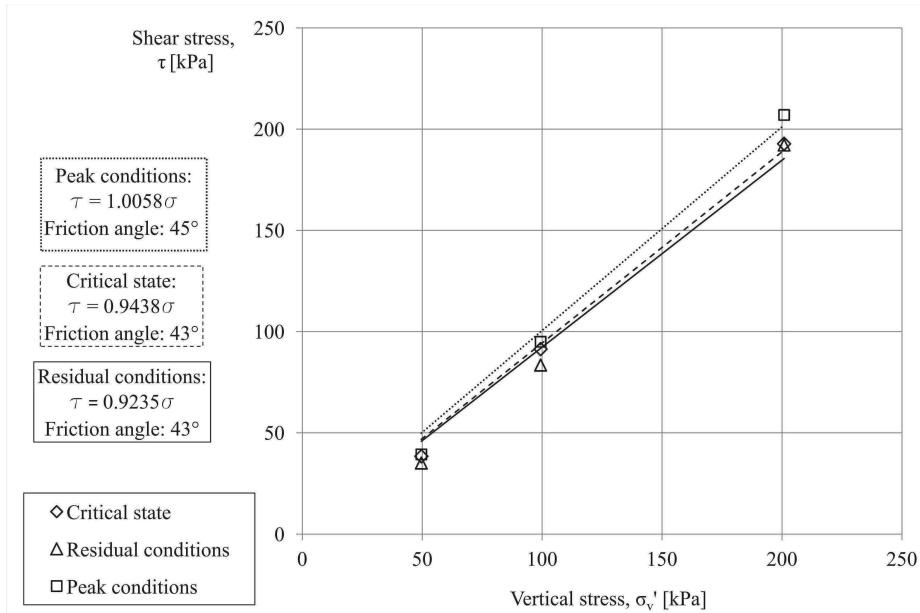The results in Fig. 5.3 indicate that the sample showed compressive behaviour, like a loose sand, for the tests performed at 50 kPa and 100 kPa confining vertical stress and dilatants behaviour, like a dense sand, for the test at 200 kPa confining vertical stress. Moreover, the sample showed a significant reduction in the critical state void ratio value with increasing vertical stresses, as a consequence of grain compressibility (or brittleness).

Finally, Fig. 5.4 reports the strength parameters of the BA based on the Mohr-Coulomb failure criterion. The friction angle values, at the peak, critical state and residual conditions of 45°, 43° and 43°, respectively, were rather high, but in agreement with other literature results (e.g. Okoli and Balafoutas, 1999; Muhunthan et al., 2004; Amaya and Amaya., 2007), while cohesion was nil.

The excellent mechanical characteristics identified for the BA could be advantageous, if the BA is used in capping systems designed with a slope to facilitate rainwater runoff. In this case, a greater safety margin against instability or failure can be expected compared to a common compacted clay liner.

The chemical composition of the BA is reported in Table 5.2. The composition is consistent with those reported in the literature (Sabbas et al., 2003; Meima and Comans, 1997; Hjelmar, 1996), with the exception of the calcium value, which is higher than that of most other BAs.

Table 5.2 – Chemical composition of the bottom ash (the concentrations refer to dry BA).

Composition of MSWI bottom ash					
Moisture	%	25.5	$C_{inorganic}$	%	1.52
Volatile matter	%	5.28	$C_{organic}$	%	0.58
Si	%	15.3	Cl	%	0.67
Ca	%	19.9	P	%	0.36
Al	%	3.72	Ba	mg kg^{-1}	1410
Mg	%	3.50	Mn	mg kg^{-1}	3616
Fe	%	2.03	Cr	mg kg^{-1}	546
Na	%	1.31	Ni	mg kg^{-1}	234
K	%	0.47	Cu	mg kg^{-1}	2894
S	%	0.49	Zn	mg kg^{-1}	2274
			Pb	mg kg^{-1}	697

The bentonite used in this study is a natural sodium bentonite with excellent purity, consisting of 99% by weight of montmorillonite, with a cation exchange capacity, CEC of 110 meq/100g. The measured K of the bentonite permeated with de-ionized water was $1.5 \cdot 10^{-11}$ m/s and the measured liquid limit and swell index were 525% and 48 mL/2g, respectively. A more detailed description of the bentonite properties can be found in Puma et al. (2011) and Puma (2012).

The BA-bentonite mixture tested in this study consisted of 10% bentonite content by dry weight basis. The mixture was prepared with a mechanical procedure starting from the dry components, i.e. the dry BA passing the 9.5 – mm sieve and the dry bentonite.

The characterization of the BA-bentonite mixture included determination of swell index according to ASTM D 5890-01, but adapting the standard procedure to analyse the extremely heterogeneous material of this mixture and of the hydraulic conductivity, using a flexible-wall permeameter according to ASTM D 5084-00.

In terms of the contaminant release of the BA-bentonite mixture, the heavy metal concentrations were determined by means of acid digestion with $HNO_3 + HCl$ and analysis of the solutions by AAS (Perkin Elmer 1100B, Uberlingen, Germany). The chlorides and other anions were determined for leachate characterization by means of ion chromatography (IC Metrohm 820 SP, Herisau, Switzerland) and the metals were determined by means of AAS or GF-AAS after acidification with concentrated HNO_3. Leaching tests were performed on the pure BA, according to EN12457-2:2002 (one-stage batch test at a liquid-to-solid ratio of 10 L/kg, using deionised water) for comparison purposes.

5.5   RESULTS AND DISCUSSIONS

5.5.1 Swelling performance of the sodium bentonite in MSWI BA-bentonite mixtures

Since, in general, a good hydraulic performance of soil-bentonite mixtures is based on a high swelling behaviour of the sodium bentonite in the presence of water, the first step of the research activity was to check whether mixing the bentonite with the BA affected the bentonite swelling capacity. As a consequence, swelling tests were performed to determinate whether the contaminants (in particular the multivalent metals) inherent in the BA were sufficient to inhibit bentonite swelling behaviour. Therefore, the standard swell index determination procedure (i.e. ASTM 5890) was adapted as follows: (1) three different mixtures were investigated, using mixing ratios, α (i.e. bentonite mass over total mass of the sample, expressed as a percentage by weight), of 5, 10 and 15%; (2) the corresponding three different masses of BA (11.3, 18 and 38 g for $\alpha = 5$, 10 and 15%, respectively) were left in 90 mL of de-ionized water for 24 h in order to allow metal release; (3) 2 g of sodium bentonite was added to each cylinder, the water level rose to the 100 mL mark and the samples were left to sediment for 16 h; and (4) the swell index values (concerning only the portion of the cylinder filled with the deposited bentonite) were recorded for each mixture.

The results showed that the bentonite swelled in all the cylinders, even when metals were released by the BA and, in particular, no substantial difference was observed between the three mixtures. The swell index values were equal to 23, 25 and 24 mL/2g for $\alpha = 5$, 10 and 15%, respectively.

The BA and sodium bentonite mixture is a dual porosity material that is basically constituted by a BA matrix in which bentonite fills the voids between the BA particles. After the voids in the BA matrix are completely filled by bentonite, the bentonite voids control hydraulic conductivity. Therefore, the BA-bentonite mixing ratio that corresponds to complete BA void filling, represents the minimum value necessary to reach a bentonite controlled hydraulic conductivity.

The dual-porosity model proposed by Revil and Cathles (1999) for a sand-shale mixture was modified to be representative of a mixture that included a swelling material, such as sodium bentonite.

According to Revil and Cathles (1999), the total porosity, n, of a mixture can be considered as the sum of two contributions: macro-porosity, consisting of the voids between the BA grains, and micro-porosity, consisting of the voids between the bentonite particles. The magnitude of the two contributions was given by Marion et al. (1992) as a function of the bentonite volume fraction, φ_v (i.e. bentonite volume over total volume of the sample), as follows:

$$\begin{cases} n = n_{BA} - \varphi_v \cdot (1 - n_b) \Leftrightarrow \varphi_v \leq n_{BA} \\ n = \varphi_v \cdot n_b \Leftrightarrow \varphi_v \geq n_{BA} \end{cases} \tag{5.1}$$

where n_{BA} and n_b are the porosity of the pure compacted BA and dry bentonite, respectively.

If $\varphi_v < n_{BA}$, the mixed bentonite partially fills the voids between the BA particles. The optimal mixing ratio, at which the macro-porosity is completely filled by bentonite and the total porosity is only a function of the micro-porosity, is found at $\varphi_v = n_{BA}$. If the optimal value is passed, the BA grains loose their connections and become a dispersed phase inside a continuous bentonite matrix.

The bentonite volume fraction, φ_v, can be expressed as a function of the physical parameters of the two components of the mixture, which can be determined from the pure materials. The following relations are obtained:

$$\varphi_v = \frac{\dfrac{\alpha}{1-\alpha} \cdot \rho_{BA} \cdot (1-n_{BA})}{\rho_b \cdot (1-n_b) \cdot \dfrac{1}{1+\varepsilon_v}} \Leftrightarrow \varphi_v \leq n_{BA}$$

(5.2)

$$\varphi_v = \frac{\alpha \cdot \rho_{BA}}{\left[\rho_b \cdot (1-n_b) \cdot \dfrac{1}{1+\varepsilon_v} \cdot (1-\alpha)\right] + \alpha \cdot \rho_{BA}} \Leftrightarrow \varphi_v \geq n_{BA}$$

where α is the mixing ratio, ρ_{BA} and ρ_b are the particle densities of the BA and bentonite, respectively, and ε_v is the volumetric strain of bentonite during saturation (which physically represents its swelling behaviour).

As already mentioned, the swelling behaviour of bentonite can be inhibited to a great extent by the presence of cations in the pore solution. If the cation concentration increases in the pore water (e.g, because of metal release by the BA), the bentonite tends to aggregate and its volumetric strain, which is achieved during saturation with pure water, gradually decreases.

The total porosity of the compacted mixture is reported as a function of the mixing ratio and for different swelling strains of the material in Fig. 5.5.

Fig. 5.5 shows that, as the bentonite swelling ability decreases, the optimal mixing ratio value tends to increase. Since a volumetric strain of 100% can be considered a maximum value for the sodium bentonite used in this study, mixing ratios of between 10% and 19% can be considered optimal. A volumetric strain value of 100% was determined by saturating bentonite at a 10 kPa effective confining stress in a flexible-wall permeameter with de-ionized water (Puma, 2012). On the basis of this result, the minimum optimal mixing ratio was evaluated to be equal to 10% and, because of the necessity of limiting the cost of bentonite for landfill capping systems, this mixing ratio value was selected for the hydraulic conductivity test.
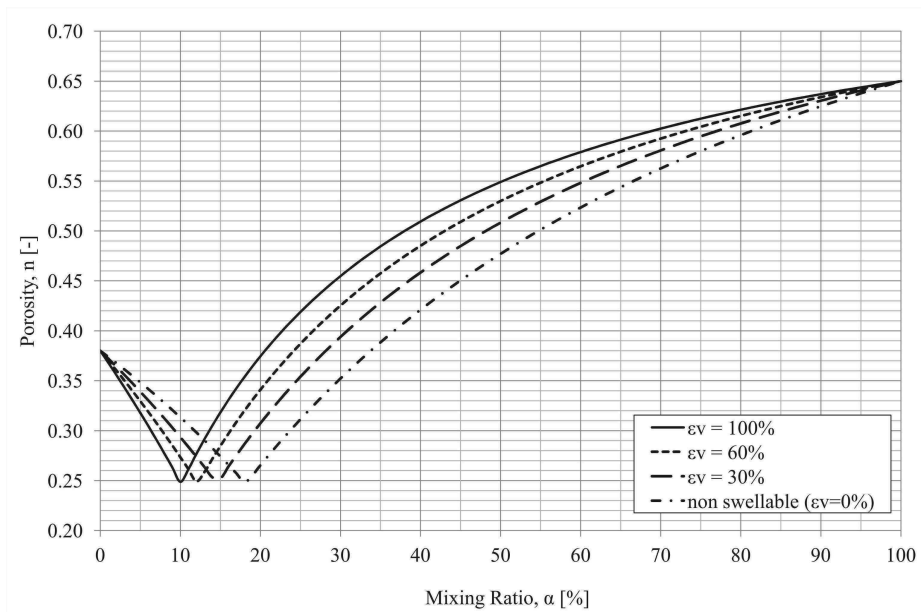
Figure 5.5 – Total porosity of the compacted mixture as a function of mixing ratio and volumetric strain of the bentonite during saturation, ε_v, (input data: porosity of the compacted bottom ash, n_{BA} = 0.38; gravimetric porosity of dry bentonite, n_b = 0.65; particle densities of the BA, ρ_{BA} = 2.56·10³ kg/m³, and bentonite, ρ_b = 2.65·10³ kg/m³).

5.5.2 Hydraulic conductivity of the BA-bentonite mixture

A flexible-wall hydraulic conductivity test was conducted to determine the hydraulic conductivity of a compacted mixture specimen according to the falling head-water/rising tail-water procedures described in ASTM D 5084-00. The specimen was compacted using a Proctor cylinder and standard compaction energy at a water content of 30% (higher than the optimal water content individuated for pure BA using the Proctor Standard method). The diameter of the specimen was 101.6 mm and the height was 60.0 mm. After specimen extrusion from the standard Proctor compaction mold, the specimen height was reduced from 116.4 mm to 60.0 mm with aim of obtaining higher hydraulic gradient and, as a consequence, a lower test duration, during the hydraulic conductivity test. The sample was back-pressured to achieve an average effective stress of 40 kPa during the saturation and the permeation phases. The test was performed using an average hydraulic gradient of 70 and terminated based on the criteria listed in ASTM D 5084-00.

The test results, reported in Fig. 5.6 as a function of time, t, and pore volume of flow, PV, indicated a steady-state hydraulic conductivity of $8 \cdot 10^{-10}$ m/s.

Figure 5.6 – Hydraulic conductivity of the compacted bentonite-bottom ash mixture as a function of time, t, and pore volumes of flow, PV.

The laboratory measured hydraulic conductivity may underestimate that of field mixture because the laboratory test does not allow the field-scale macro-heterogeneity of a hydraulic barrier to be taken into account. In spite of this, the hydraulic conductivity value obtained was more than one order of magnitude lower than that required by the Italian legislation pertaining to landfill covers (i.e. $K \leq 10^{-8}$ m/s). Therefore, the studied BA-bentonite mixture appears to be a suitable cover material based on hydraulic conductivity although field testing would be required for verification.

5.5.3 Leachate characterization

The results concerning the leachate quality of the BA-bentonite mixture are compared with the results obtained from the pure BA (particle diameter < 9.5 mm) and with the Italian legislation limits for waste leachate in non-hazardous solid waste landfills in Table 5.3. The metal concentrations of the leachate collected during the hydraulic conductivity test are based on a liquid volume corresponding to 1 PV (1 PV $\approx$ 0.3 L for the specimen used in the test). Since the dry mass of the specimen is   0.49 kg, the solid/liquid ratio for the BA-bentonite mixture characterization is very low, i.e. 0.6 L/kg. The BA leachate characterization and the Italian legislation limits reported in Table 5.3 refer to EN12457-2:2002, which requires a solid/liquid ratio of 10 L/kg in the leaching tests. As a consequence, the leachate characterization performed during the hydraulic conductivity test corresponds to the most unfavourable condition.

Table 5.3 – Chemical characterization of the leachate from a bottom ash-bentonite mixture and pure BA compared with the Italian limits pertaining to landfilling of waste in non-hazardous solid waste landfills.

	units	Leachate from the hydraulic conductivity test on BA-bentonite mixture	Leachate from leaching tests on pure BA[1]	Italian legislation limits (DM 27/09/2010) for waste leachate in non-hazardous solid waste landfills[1]
pH		10.25	11.69	$\geqslant 6$
Electrical conductivity	μScm^{-1}	1660	2209	-
Chlorides	mgL^{-1}	210	148	< 2500
Sulphates	mgL^{-1}	214		< 5000
Nitrate	mgL^{-1}	1.9		-
Ca	mgL^{-1}	1.3		-
Al	mgL^{-1}	153.7		-
Fe	mgL^{-1}	9.6		-
Cd	μgL^{-1}	<0.25		< 100
Cr	μgL^{-1}	100		< 1000
Cu	μgL^{-1}	117	580	< 5000
Pb	μgL^{-1}	25	100	< 1000
Zn	μgL^{-1}	12		< 5000
Ni	μgL^{-1}	<1.5		< 1000

[1] based on EN 12457

The leachate collected from the permeameter presented similar electrical conductivity, pH and chloride concentration values to those of the BA leachate. The heavy metal concentration was very low, and was always less than the landfilling limit values established in Italian legislation. Consequently, the use of BA-bentonite mixture in landfill capping systems does not result in any additional risk since the toxic compounds are released inside the landfill.

5.6   CONCLUSIONS

MSWI BA is made up of heterogeneous sand-like material that presents several physical and mechanical advantages, compared to natural filling materials, but does not show the hydraulic conductivity necessary to satisfy Italian standard requirements for landfill cover hydraulic barriers. For this reason, the possibility of mixing BA with a natural material that would be able to achieve a relatively low hydraulic conductivity, such as natural sodium bentonite, was considered in this study, in order to minimize infiltration of precipitation in landfill cover systems.

The preliminary BA characterisation has highlighted that the compacted dry unit weight of the BA is generally lower than the average value that characterizes most conventional fill materials and this could be considered advantageous for a landfill cover system because of the low bearing capacity and high tendency to long term settlement of the waste. Moreover, direct shear tests have shown the excellent mechanical characteristics of the BA samples, and this is an advantage for their use in capping systems designed with a certain slope to facilitate rainwater runoff, because, in this case, greater safety is guaranteed against instability or failure.

As far as the mixing with bentonite, which is necessary to reduce the hydraulic conductivity of the pure BA, is concerned, a detrimental effect on the swelling ability of Na-bentonite may occur because of the release of calcium from BA. However, the results obtained in the swell index tests have shown that the bentonite used in this study swelled even when contaminants were released by BA, and that there were no substantial differences between the three BA-bentonite mixtures: $\alpha=5$; 10; 15%.

A mixture with a mixing ratio, α, of 10% was selected for the hydraulic conductivity test on the basis of the results obtained with the dual-porosity model modified to be representative of a mixture including a swelling material. The obtained results show a steady-state hydraulic conductivity of $8 \cdot 10^{-10}$ m/s for the mixture, which is more than one order of magnitude lower than that required by Italian legislation concerning landfill covers.

The chemical behaviour of the BA and BA-bentonite mixture is similar. As far as heavy metal release (lead and copper) is concerned, the BA-bentonite mixture has shown very low concentrations in the leachate and the values are lower than those obtained for the fine fraction of the BA. This evidence suggests a positive effect, due to the heavy metal absorption on bentonite, which decreases the potential release of contaminants from BAs, but does not inhibit the bentonite swelling behaviour, as shown in the swell index tests. Moreover, the use of BA-bentonite mixture in capping systems does not increase the release of contaminants from the landfill. Indeed, if the mixture is placed in the cover liner, the heavy metals are released from BA inside the landfill without exceeding the concentration limits of Italian legislation.

REFERENCES

Abichou, T., Benson, C.H., and Edil, T.B. (2002a). Foundry green sands as hydraulic barriers: Field study. Journal of Geotechnical and Geoenvironmental Engineering, ASCE, **128**(3), 206-215.

Abichou, T., Benson, C.H., and Edil, T.B. (2002b). Microstructure and hydraulic conductivity of simulated sand-bentonite mixtures. Clays and Clay Minerals, **50**(5), 537-545.

Alston, C., Daniel, D.E., and Devroy, D.J. (1997). Design and construction of sand-bentonite liner for effluent treatment lagoon, Marathon, Ontario. Canadian Geotechnical Journal, **34**(6), 841-852.

Appendino P., Ferraris M., Matekovits I., Salvo M. (2004). Production of glass-ceramic bodies from the bottom ashes of municipal solid waste incinerators. Journal of European Ceramic Society (24), 803-810.

Amaya, P. J., Amaya, A. J. (2007). The use of bottom ash in the design of dams. World of Coal Ash (WOCA), Covington, Kentucky, USA.

Birgisdottir H., Pihl K.A., Bhander G., Hauschild M.Z., Christensen T. H. (2006). Environmental assessment of road constructed with and without bottom ash from municipal solid waste incineration. Transportation Research Part D (11), 358-368.

Boccaccini, A.R., Petitmermet, M., Intermantel, E.W., 1997. Glass–ceramics from municipal incinerator fly ash. Ceramic Bulletin (76), 75–78.

Castelbaum, D. and Shackelford, C.D. (2009). Hydraulic conductivity of bentonite slurry mixed sands. Journal of Geotechnical and Geoenvironmental Engineering, ASCE, **135**(12),1941-1956.

Chandler, A.J., Eighmy, T.T., Hartlén, J., Hjelmar, O., Kosson, D.S., Sawell, S.E., van der Sloot, H.A., Vehlow, J. (1997). Municipal Solid Waste Incinerator Residues. Studies in Environmental Science, 67. IAWG, Elsevier Science, Amsterdam, The Netherlands.

Chapuis, R.P., Lavoie, J., and Girard, D. (1992). Design, construction, performance, and repair of the soil-bentonite liners of two lagoons. Canadian Geotechnical Journal, **29**(4), 638-649.

Creek, D.N. and Shackelford, C.D. (1992). Permeability and leaching characteristics of fly ash liner materials. Soils, Geology, and Foundations, Geoenvironmental and Engineering Properties of Rock, Soil, and Aggregate, Transportation Research Record 1345, TRB, NRC, National Academy Press, Washington, DC, 74-83.

Dominijanni, A., Genon, G., Luciani, P., Maggiorotto, M., Manassero, M, Marchese, F., Puma, S., Soldi, G.L., Zanetti, M.C. (2009). Landfilling and reuse of bottom ashes from refuse derived fuel and municipal solid waste incineration. Proceedings Sardinia 2009, Twelfth International Waste Management and Landfill Symposium, Cagliari, Italy; 5 - 9 October 2009.

Ebina, T., Minja, R.J.A., Nagase, T., Onodera, Y., and Chatterjee, A. (2004). Correlation of hydraulic conductivity of clay-sand compacted specimens with clay properties. Applied Clay Science, **26**(1), 3-12.

Eurostat (2012). European Commission. Environmental Data Centre on Waste.

 http://epp.eurostat.ec.europa.eu/portal/page/portal/waste/data/main_tables

Forteza, R., Far, M., Seguí, C., Cerdá, V. (2004). Characterization of bottom ash in municipal solid waste incinerators for its use in road base. Waste Management, **24**(9), 899-909.

Garlanger, J.E., Cheung, F.K., Bishar, S.T. (1987). Quality control testing for a sand-bentonite liner. Geotechnical Practice for Waste Disposal '87. R.D. Woods, ed. ASCE, Reston, Va. 488-499.

Gipson, A.H., Jr. (1985). Permeability testing on clayey soil and silty sand-bentonite mixture using acid liquor. Hydraulic Barriers in Soil and Rock, ASTM STP 874, A.I. Johnson, R.K. Frobel, N.J. Cavalli, and C.B. Pettersson, eds., ASTM, West Conshohocken, 140-54.

Gleason, M.H., Daniel, D.E., and Eykholt, G.R. (1997). Calcium and sodium bentonite for hydraulic containment applications. Journal of Geotechnical and Geoenvironmental Engineering, ASCE, **123**(5), 438-445.

Goh, A.T.C., Tay, J.H. (1993). Municipal solid-waste incineration fly ash for geotechnical applications. Journal of Geotechnical Engineering, **119**(5), 811-825.

Haug, M.D. and Wong, L.C. (1992). Impact of molding water content on the hydraulic conductivity of compacted sand-bentonite. Canadian Geotechnical Journal, **29**(2), 253-262.

Haug, M.D. and Bolt-Leppin, B. (1994). Influence of polymers on the hydraulic conductivity of marginal quality bentonite-sand mixtures. Hydraulic Conductivity and Waste Contaminant Transport in Soil, ASTM STP 1142, D.E. Daniel and S.J. Trautwein, eds., ASTM, West Conshohoken, PA, 407-421.

Hjelmar, O. (1996) Disposal strategies for municipal solid waste incineration residues. Journal of Hazardous Materials, 47, 345-368.

Howell, J.L. and Shackelford, C.D. (1997). Hydraulic conductivity of sand admixed with processed clay mixtures. Proceedings, 14th International Conference on Soil Mechanics and Foundation Engineering, Hamburg, Germany, Sept. 6-12, 1997, A. A. Balkema, Rotterdam, The Netherlands, Vol. 1, 307-310.

Izquierdo, M., Vazquez, E., Querol, X., Barra, M., López, Á., Plana, F. (2001). Use of bottom ash from municipal solid waste incineration as a road material. International Ash Utilization Symposium, Centre for Applied Energy Research, University of Kentucky, Paper #37.

Izquierdo M., Lopez-Soler A., Ramonich E.V., Barra M. & Querol X. (2002). Characterisation of bottom ash from municipal solid waste incineration in Catatonia. Journal of Chemical Technology and Biotechnology **77**, 576-583.

Kamon, M., Katsumi, T. And Sano, Y. (2000). MSW fly ash stabilized with coal ash for geotechnical application. Journal of Hazardous Materials **76**, 265-283.

Kaoser, S., Barrington, S., Elektorowicz, M., and Ayadat, T. (2006). The influence of hydraulic gradient and rate of erosion on hydraulic conductivity of sand-bentonite mixtures. Soil and Sediment Contamination, **15**(5), 481-496.

Kenney, T.C., van Veen, W.A., Swallow, M.A., and Sungaila, M.A. (1992). Hydraulic conductivity of compacted bentonite-sand mixtures. Canadian Geotechnical Journal, **29**(3), 364-374.

Lancellotta, R. (2009). Geotechnical Engineering, Second Edition. Taylor & Francis Ed., New York.

Lundgren, T. A. (1981). Some bentonite sealants in soil mixed blankets. Proceedings, 10th International Conference on Soil Mechanics and Foundation Engineering, Stockholm, Sweden, June 15-19, A. A. Balkema, Rotterdam, The Netherlands, Vol. 2, 349-354.

Mangialardi, T., (2001). Sintering of MSW fly ash for reuse as a concrete aggregate. Journal of Hazardous Materials (B87), 225–239.

Marion, D., Nur, A., Yin, H., Han, D. (1992). Compressional velocity and porosity in sand-clay mixtures. Geophysics, Volume 57, 554-563.

Meima, J.A., & Comans, R.N.J. (1997). Geochemical modelling of weathering reactions in municipal waste incinerator bottom ash. Environmental Science Technology, **31**, 1269-1276.

Mollins, L.H., Stewart, D.I., and Cousens, T.W. (1996). Predicting the properties of bentonite-sand mixtures. Clay Minerals, **31**(2): 243-252.

Monteiro, R.C.C., Figueiredo, C.F., Alendouro, M.S., Ferro, M.C., Davim, E.J.R., Fernandes, M.H.V. (2008). Characterization of MSWI bottom ashes towards utilization as glass raw material. Waste Management, **28**, 1119-1125.

Muhammad, N., Ashmawy, A. K. (2003). Compatibility of incinerator ash-soil mix as an alternative material for landfill liners and covers. Master's Thesis, University of South Florida, Tampa, Florida.

Muhunthan, B., Taha, R., Said, J. (2004). Geotechnical engineering properties of incinerator ash mixes. Journal of the Air & Waste Management Association, **54** (8), 985-991.

Okoli, R.E., Balafoutas, G. (1999). Bottom ash from sludge cake as a barrier material to pollutant migration in landfills. Waste Management and Research, **17**, 288-295.

O'Sadnick, D.L., Simpson, B.E., and Kasel, G.K. (1995). Evaluation and performance of a sand-bentonite liner. Geoenvironment 2000, Y.B. Acar, and D.E. Daniel, eds, ASCE, Reston, Va., 688-701.

Plescia, P., Paolini, G., Tocino, M.A., Furia, G. (2006). Scorie pesanti da incenerimento dei rifiuti solidi urbani. Recycling, November 2006.

Poran, C.J., Ahtchi-Ali, F., 1989. Properties of solid waste incinerator fly ash. Journal of Geotechnical Engineering, **115**(8), 1119–1133.

Puma, S., Dominijanni, A., Manassero, M., Toncelli, D., Trotta, F. and Zanetti, M. (2011). Hydraulic performance of a natural bentonite GCL in inorganic solutions and polymer treatment proposal to prevent degradation in long term landfill conditions. Proceedings Sardinia 2011, 13th International Waste Management and Landfill Symposium. CISA Publisher, Cagliari.

Puma, S. (2012). Improvement of bentonite barriers for pollutant containment. PhD Thesis. Politecnico di Torino. (in preparation).

Revil, A., Cathles, L. M. III (1999). Permeability of shaly sands. Water Resources research, **35**, 651-662.

Rogbeck, J., Hartlen, J. (1996) Ash gravel – a material for recycling. Waste Management, **16**(1–3), 109–12.

Romero, M., Ma Rincon, J., Rawlings, R.D., Boccaccini, A.R., 2001. Use of vitrified urban incinerator waste as raw material for production of sintered glass–ceramics. Materials Research Bulletin **36**, 383–395.

Sabbas, T., Polettini, A., Pomi, R., Astrup, T., Hjelmar, O., Mostbauer, P., Cappai, G., Magel, G., Salhofer, S., Speiser, C., Heuss-Assbichler, S., Klein, R., & Lechner,

P. (2003). Management of municipal solid waste incineration residues. Waste Management, **23**, 61-88.

Sakai, S., Hiraoka, M., 2000. Municipal solid waste incinerator residue recycling by thermal processes. Waste Management 20, 249–258.

Sällfors, G. and Öberg-Högsta, A.-L. (2002). Determination of hydraulic conductivity of sand-bentonite mixtures for engineering purposes. Geotechnical and Geological Engineering, **20**(1), 65-80.

Shackelford, C.D. and Glade, M. (1994). Constant-flow and constant-gradient hydraulic conductivity tests on sand-bentonite-fly ash mixtures. Hydraulic Conductivity and Waste Contaminant Transport in Soil, D.E. Daniel and S.J. Trautwein, Eds., STP 1142, ASTM, West Conshohoken, PA, 521-545.

Stern, R. T., Shackelford, C. D. (1998). Permeation of sand-processed clay mixtures with calcium chloride solutions. Journal of Geotechnical and Geo-environmental Engineering, **124**(3), 231-241.

Teachavorasinskun, S. and Visethrattana, K. (2006). Local hydraulic resistance of compacted sand-bentonite mixture. Géotechnique, **56**(7), 511-516.

Wang, K.S., Chiang, K.Y., Perng, J.K., Sun, C.J., (1998). The characteristics study on sintering of municipal solid waste incinerator ashes. Journal of Hazardous Materials **59**, 201–210.

Wang, K.S., Sun, C.J., Yeh, C.C., (2002). The thermotreatment of MSW incinerator fly ash for use as an aggregate: a study of the characteristics of size-fractioning. Resources, Conservation and Recycling **35**, 177–190.

Wiles, C. (1996). Municipal solid waste combustion ash: state of the knowledge. Journal of Hazardous Materials, **47**, 325–344.

Xue, Y., Hou, H., Zhu, S., Zha, J. (2009). Utilization of municipal solid waste incineration ash in stone mastic asphalt mixture: pavement performance and environmental impact. Construction and Building Materials **23**, 989-996.

FINITE DIFFERENCE MODELLING OF DIFFUSIVE FLUX OF CALCIUM THROUGH A BENTONITE BARRIER IN IN-SITU CONDITIONS

The evidence of the strong degradation induced in the hydraulic performances of sodium bentonite barriers by the cation exchange phenomenon has been highlighted in the previous chapters. This experimental result underlines the need to study the temporal development of the cation exchange phenomenon with the aim to compare that to the period in which landfill barrier performances have to be guaranteed in in-situ conditions.

The mathematical study developed in this chapter is focused on the evaluation of the role of the diffusive component of Calcium flux in the cation exchange phenomenon which can develop in a sodium bentonite barrier, placed in an environment inexorably rich in chemical compounds containing soluble Calcium (i.e. the natural soil, the aquifer, the drainage layer saturated with waste leachate or raining water).

6.1 ENGINEERING PROBLEM.

6.1.1. Use of GCLs in landfill.

The dry GCL, containing sodium bentonite (NaB), is unrolled in situ during the construction of the landfill bottom liner and it can be, eventually, saturated with tap water before being covered with a thin layer of soil, aimed at protecting the geosynthetic, or, if a composite liner has to be built, with a geomembrane (GM).

In Figure 6.1 some photographs are reported, aimed at describing the main installation phases of a GCL in a landfill cover or bottom liner.

In landfill conditions, the bentonite, contained inside the GCL, stands in an environment inexorably rich in chemical compounds containing soluble Calcium, such as the foundation natural soil (that, if saturated, corresponds to the aquifer) or the drainage layer, saturated by the leachate of the wastes or by the raining water.

Figure 6.1 – Main installation phases of a GCL in a landfill cover or bottom liner.

In Figure 5.2 two schematic vertical cross-sections are reported, respectively of a landfill cover system and a landfill bottom liner. In landfill conditions, bentonite generally stands on both side in contact with soluble Calcium.

6.1.2 Simplification of the problem: GCL inside a landfill barrier.

The problem of the NaB GCL placed inside a landfill barrier can be simplified through considering a thin bentonite layer, approximately 10 mm thick, posed between two reservoirs containing the pore solutions of the leachate drainage layer, the raining water drainage layer or the foundation soil.

The whole system is considered perfectly saturated.

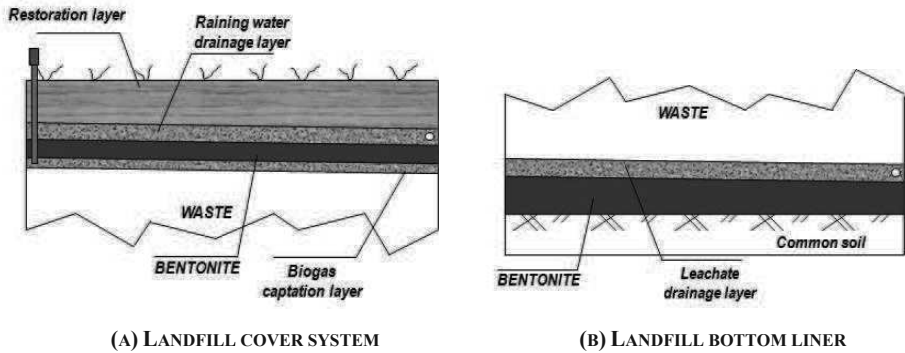**(A) LANDFILL COVER SYSTEM**   **(B) LANDFILL BOTTOM LINER**

Figure 6.2 – Schematic vertical cross-sections.

In the most general case, reported in Figure 6.3, both the hydraulic gradient and the concentration gradient do exist. Consequently, Calcium flux in the system consists in the sum of two components:

(1) the <u>advective component to Calcium flux</u>, due to the dragging caused by the volumetric water flux from the upper to the lower reservoir;

(2) the <u>diffusive component to Calcium flux</u> from outside to inside the bentonite layer (induced by the concentration gradient).
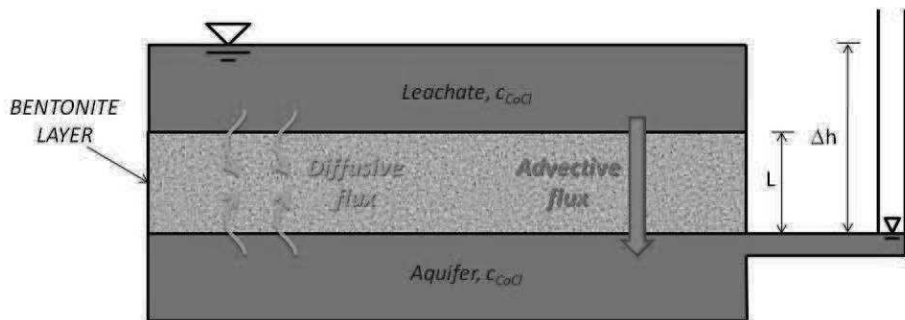

Figure 6.3 – Schematic presentation of the problem in the most general case (considering both the hydraulic and the concentration gradient).

6.1.2.1 Advective flux approach (Shackelford, 2005).

Considering only the <u>advective flux</u>, Shackelford (2005) studied the development of cation exchange phenomenon in a GCL and its consequent long term hydraulic

conductivity. The problem approach adopted by Shackelford (2005) rests on the results of several hydraulic conductivity tests carried out using different $CaCl_2$ concentrations in the permeation solution. Jo et al. (2005) attribute the longer test duration of the tests performed using solution with the lower $CaCl_2$ concentrations to the lower rate of Ca^{2+} mass loading such that the time required for equilibrium exchange with the Sodium initially in NaB increases.

Since in the laboratory, when permeability tests were performed, higher hydraulic gradients (i.e. i $\approx$ 200) are used, Shackelford (2005) states that the time required to achieve chemical equilibrium (i.e. the completion of cation exchange phenomenon) in field conditions, where much lower hydraulic gradients are expected, is likely to be significantly greater.

Since the time required to achieve chemical equilibrium is a function of Calcium mass loading rate, it is mainly influenced by two parameters:

(1) $CaCl_2$ concentration in the permeant solution;

(2) the Darcian velocity, q, that, for the same material (that means, for the same hydraulic conductivity coefficient, k) is just a function of the hydraulic gradient, i.

Assuming that temporal trend of the hydraulic conductivity in the field is the same as that in the laboratory (i.e. for the same initial and boundary conditions) but it is extended over a longer duration, Shackelford (2005) found a correlation that scales, for any value of $CaCl_2$ concentration in the permeant solution, the time required to achieve chemical equilibrium measured in laboratory to the field conditions. The results obtained for $CaCl_2$ concentration equal to 20 mM are reported in Figure 6.4.
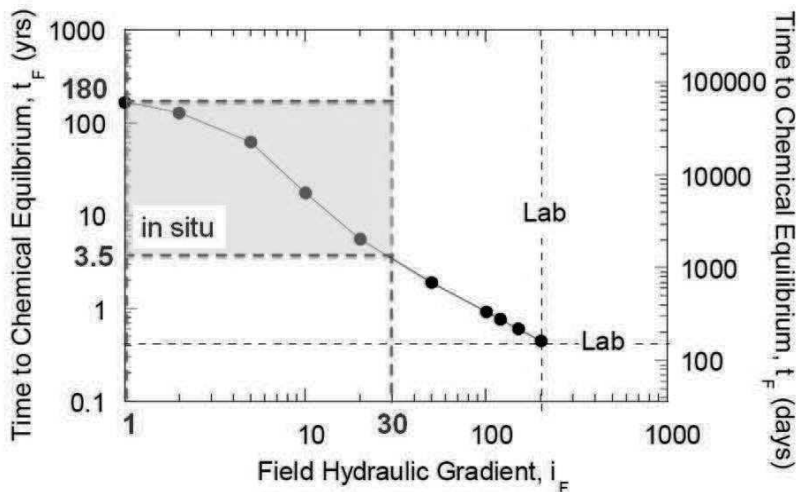
Figure 6.4 – Estimated correlation between times to achieve chemical equilibrium and hydraulic gradient in the field based on the results of a laboratory test data for a GCL permeated with a 20 mM $CaCl_2$ solution under a hydraulic gradient of 200 (modified from Shackelford, 1993).

Figure 6.4 is modified from Shackelford (2005) to highlight that for the typical field hydraulic gradients, ranging from 30 (i.e. a leachate hydraulic level equal to 30 cm contained inside the drainage layer) to 1 (i.e. infiltration flux), the corresponding times to achieve chemical equilibrium range between 3.5 and 180 years. Moreover, it is important to underline that a 20 mM solution can correctly represent a typical Calcium concentration in the leachate while it represent an upper limit for common Calcium concentrations in soil.

The study developed by Shackelford (2005) highlights a strong dependence of the value of time necessary to reach chemical equilibrium on the applied hydraulic gradient. Moreover, for a hydraulic gradient lower than 10, which may correspond to a correct working configuration of the landfill leachate drainage system, the time to achieve chemical equilibrium can be quantified in some tens of years. This last result, even if it does not fully satisfy the typical long term landfill requirements (i.e. 50-70 years), can be considered a good result in term of performance maintaining.

6.1.2.2 Diffusive flux approach.

A great simplification is assumed in the work of Shackelford (2005): the contribution of the diffusive Calcium flux from the surrounding soil to the NaB is neglected.

Especially when low permeability material, such as Sodium bentonite ($k \approx 10^{-11}$ m/s), and field conditions (low value of i) are considered, the volumetric water flux across the bentonite layer may decrease so much to result unimportant if compared with the contribution of the diffusive flux induced by the Calcium concentration gradient existing from outside to inside the GCL.

For this reason, the role of the diffusive contribution to the Calcium supply inside the NaB layer is analyzed in this chapter.

The following cases are analyzed:

(A) A 10 mm Sodium bentonite layer standing between two reservoirs containing the same concentration of Calcium Chloride (see Figure 6.5).

(B) A composite barrier given by a 10 mm Sodium bentonite layer and a Geomembrane (GM) posed above. The barrier stands between two reservoirs containing the same concentration of $CaCl_2$ but the GM completely inhibits the diffusive Calcium flux from the upper reservoir to the bentonite layer (see Figure 6.6).
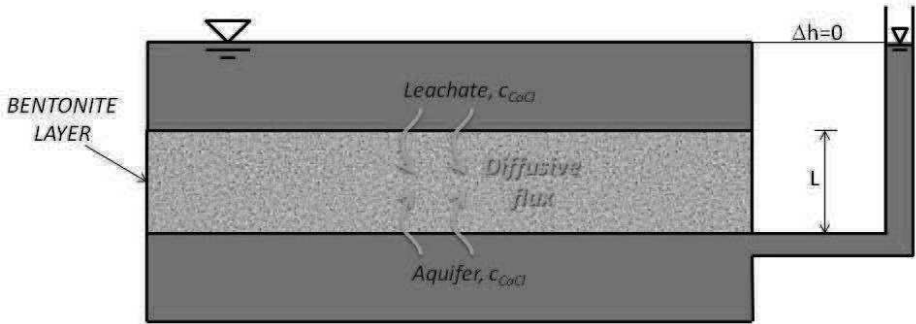

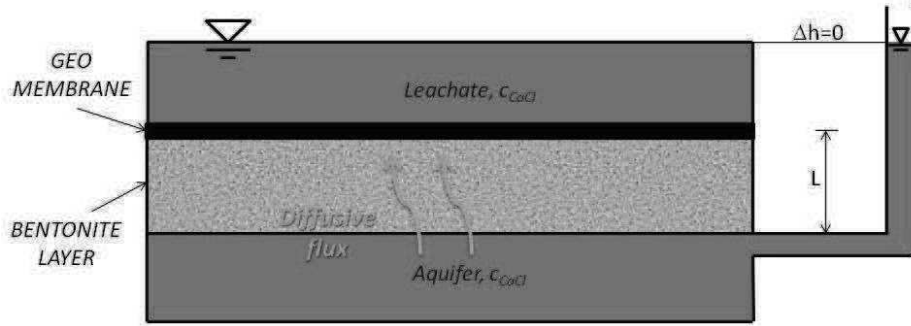Figure 6.5 – Scheme of the case A: 10 mm Sodium bentonite layer.

Figure 6.6 – Scheme of the case B: composite liner = GM + 10 mm Sodium bentonite layer.

6.2. FROM THE ENGINEERING PROBLEM TO THE MATHEMATICAL PROBLEM

6.2.1. Porous medium characteristics.

Bentonite soils behaving as semipermeable porous media may be modelled as continuum mixtures consisting of a solid phase, an interstitial solvent (generally, water) and N different species of ions. The total number of constituents of the soil is N+2.

The volume fractions of the components of the mixture are defined as:

$$n_a = \frac{V_a}{V} \qquad a = s, w, 1, 2, ..., N \tag{6.1}$$

where a (= s,w, 1,2,…, N) denotes the components (solid, water, ion-species 1, ion-species 2,…, etc.) within the bentonite, V_a is the volume occupied by the a-th component and V is the Representative Elementary Volume (REV). We assume that the bentonite is saturated: thus, the summation of the volume fractions of each component is equal to unity, that is:

$$\sum_a n_a = 1 \tag{6.2}$$

Assuming the pore solution sufficiently diluted, the volume fraction of the ions may be neglected and the condition *(6.2)* reduces to:

$$n_w + n_s = 1 \tag{6.3}$$

We will indicate the volume fraction of the water simply as the porosity, n, and the volume fraction of the solid phase, as (1-n).

The solid phase of bentonite is charged. The charge is supposed arising from the isomorphous substitution of lower-valence cations for higher-valence cations within the structure and is negative (see paragraph 1.1).

The charge characterizing the solid phase is taken into account as a molar concentration of the solid skeleton electric charge (per unit volume of pore), $\overline{c}_{sk}$ uniformly distributed within the porous medium, assumed proportional to the cation exchange capacity, CEC, and inversely proportional to the void ratio, e, (Dominijanni, 2005), as already described in paragraph 2.6.3:

$$\overline{c}_{sk} = \phi_X CEC \rho_s \frac{1}{e} = \frac{\overline{c}_{sk,0}}{e} \tag{6.4}$$

6.2.2. Momentum Balance Equations.

The momentum balance equations were obtained by Dominijanni (2005) for the solute and solvent component inside a porous medium. The derivation of the fundamental equation is reported in the following.

The balance of momentum for the generic component of the mixture is given by:

$$\rho_a \vec{a}_a = \nabla \cdot \hat{T}_a + \vec{F}_a - \vec{m}_a \qquad a = s, w, 1, 2, ..., N \tag{6.5}$$

Where:

$\vec{a}_a$ is the acceleration of the a-th component,

$\hat{T}_a$ is the stress tensor,

$\vec{F}_a$ is the external force per unit volume acting on the a-th component,

$\vec{m}_a$ is the interaction force between the a-th component and the other components of the mixture, given by:

$$\vec{m}_a = \sum_{\substack{b=1 \\ b \neq a}}^{N+1} \vec{m}_{ab} \tag{6.6}$$

For the Fluid Phase:

The following hypothesis may be assumed:

I. the inertia of each component is neglected;

II. the viscosity of each component of the fluid phase does not explicitly enter into the expression for the stress of the component, so that the stress of each component is that of a *perfect fluid*:

$$\nabla \cdot \hat{T}_b = -\nabla(n\bar{u}_b) = -n\nabla\bar{u}_b - \bar{u}_b \nabla n \qquad b = w,1,2,\dots,N \tag{6.7}$$

III. the interaction force of each component with the others may be decomposed in two terms:

$$\vec{m}_b = -\bar{u}_b \nabla n + \vec{m}'_b \qquad b = w,1,2,\dots,N \tag{6.8}$$

IV. the transport is uni-dimensional in the direction x.

The resulting momentum balance equation *(6.5)* for the fluid phase may be written as follows:

$$\underbrace{\rho_b \vec{a}_b = 0}_{\text{Hp. I}} + \left(-n\frac{d\bar{u}_b}{dx} \underbrace{- \bar{u}_b \frac{d\bar{u}_b}{dx}}_{\text{Hp. II}} \right) + \vec{F}_b - \overbrace{\left(-\bar{u}_b \frac{d\bar{u}_b}{dx} + \sum_{\substack{a=1 \\ a\neq b}}^{N+1} \vec{m}'_b \right)}^{\text{Hp. III}}$$

$$-n\frac{d\bar{u}_w}{dx} + F_w = \sum_{i=1}^{N} m'_{wi} + m'_{ws} \qquad \text{for the solvent} \tag{6.9a}$$

$$-n\frac{d\bar{P}_i}{dx} + F_i = m'_{iw} + \sum_{\substack{j=1 \\ j\neq 1}}^{N-1} m'_{ij} + m'_{is} \qquad i = 1,2,\dots,N \qquad \text{for the solute} \tag{6.9b}$$

V. Neglecting the gravitational force, the only external force acting on the components of the fluid phase is the electric one:

$$F_w = 0 \tag{6.10a}$$

$$F_i = -nz_i F\bar{c}_i \frac{d\bar{\varphi}}{dx} \quad i = 1,2,\ldots, N \tag{6.10b}$$

Where:

z_i is the electro-chemical valence of the i-th ion,

F is the Faraday constant,

$\bar{c}_i$ is the concentration of the i-th ion within the semipermeable porous medium,

$\bar{\varphi}$ is the electric potential within bentonite.

VI. The binary interaction forces may be assumed to be viscous forces, proportional to the relative velocity and to the concentrations of the components of the mixture:

$$m'_{ws} = n\alpha(v_w - v_s) \tag{6.11a}$$

$$m'_{is} = n\beta_{is}\bar{c}_i(v_i - v_s) \quad i = 1,2,\ldots, N \tag{6.11b}$$

$$m'_{wi} = n\zeta_{wi}\bar{c}_w\bar{c}_i(v_w - v_i) = nf_{wi}\bar{c}_i(v_w - v_i) \quad i = 1,2,\ldots,N \tag{6.11c}$$

$$m'_{iw} = n\zeta_{iw}\bar{c}_i\bar{c}_w(v_i - v_w) = nf_{iw}\bar{c}_i(v_i - v_w) \quad i = 1,2,\ldots,N \tag{6.11d}$$

$$m'_{ij} = n\zeta_{ij}\bar{c}_i\bar{c}_j(v_i - v_j) \quad i,j = 1,2,\ldots,N \tag{6.11e}$$

where $\alpha, \beta_{is}, f_{wi}, f_{iw}, \zeta_{ij}$ are friction coefficients.

VII. Supposing that the interactions between the components of the fluid phase are binary:

$$f_{wi} = f_{iw} \quad i = 1,2,\ldots, N \tag{6.12a}$$

$$\zeta_{ij} = \zeta_{ji} \quad i,j = 1,2,\ldots, N \tag{6.12b}$$

Inserting hypothesis *(6.10)*, *(6.11)* and *(6.12)* in equations *(6.9)* we obtain:

$$-\frac{d\bar{u}_w}{dx} = \sum_{i=1}^{N} f_{wi}\bar{c}_i(v_w - v_i) + \alpha(v_w - v_s) \tag{6.13a}$$

$$-\frac{d\overline{P}_i}{dx} - z_i \overline{c}_i F \frac{d\overline{\phi}}{dx} = f_{wi}\overline{c}_i(v_i - v_w) + \sum_{\substack{j=1 \\ j\neq 1}}^{N-1}\left[\zeta_{ij}\overline{c}_i\overline{c}_j(v_i - v_j) + \beta_{is}\overline{c}_i(v_i - v_s)\right]$$

$$i = 1,2,...,N$$

(6.13b)

VIII. If the pore solution is dilute, or rather, if the ion species are sufficiently rarefied, the prevalent interaction force that they exchange with the other components of the mixture is that with the water: the interaction forces between two different ions and between ions and solid may be neglected in comparison with the interaction force between ions and water.

$$f_{wi} \gg \zeta_{ij}$$

$$f_{wi} \gg \beta_{is}$$

The resulting momentum balance equations are:

$$-\frac{d\overline{u}_w}{dx} = \sum_{i=1}^{N} f_{wi}\overline{c}_i(v_w - v_i) + \alpha(v_w - v_s)$$

(6.14a)

$$-\frac{d\overline{P}_i}{dx} - z_i\overline{c}_i F\frac{d\overline{\phi}}{dx} = f_{iw}\overline{c}_i(v_i - v_w) \quad i = 1,2,...,N$$

(6.14b)

6.2.3. Solute transport equation for a semi-permeable porous medium.

The solute transport equation was obtained by Dominijanni (2005) for a semi-permeable porous medium in the case of zero electric current. The derivation of the fundamental equation is reported in the following.

The volumetric flux of solvent is given by:

$$q = n(v_w - v_s) \qquad (6.15)$$

The momentum balance equation for the whole system is derived summing equations *(6.14a)* and *(6.14b)*:

$$-\frac{d\overline{u}_w}{dx} - \sum_{i=1}^{N} \frac{d\overline{P}_i}{dx} - \left(\sum_{i=1}^{N} z_i \overline{c}_i \right) F \frac{d\overline{\varphi}}{dx} = \alpha(v_w - v_s) \qquad (6.16)$$

Substituting *(6.16)* in *(6.15)* we obtain:

$$q = -\frac{n}{\alpha} \cdot \left[\frac{d\overline{u}_w}{dx} + \sum_{i=1}^{N} \frac{d\overline{P}_i}{dx} - \left(\sum_{i=1}^{N} z_i \overline{c}_i \right) F \frac{d\overline{\varphi}}{dx} \right] \qquad (6.17)$$

We need to observe that for a semi-permeable porous medium the total pressure is the sum of the partial pressures of the components of the fluid phase:

$$\overline{u} = \overline{u}_w + \sum_{i=1}^{N} \overline{P}_i \qquad (6.18)$$

and that the electro-neutrality condition is given by:

$$\sum_{i=1}^{N} z_i \overline{c}_i + \varpi \overline{c}_{sk} = 0 \qquad (6.19)$$

where ϖ is the sign of the fixed charge (for clays with a negative fixed charge, $\varpi = -1$).

Finally, substituting equations *(6.18)* and *(6.19)* in equation *(6.17)* we obtain the volumetric flux or Darcy velocity in a semi-permeable porous medium:

$$q = -\frac{n}{\alpha}\left(\frac{d\overline{u}}{dx} - \varpi\overline{c}_{sk}F\frac{d\overline{\varphi}}{dx}\right) = -nd_h\left(\frac{d\overline{u}}{dx} - \varpi\overline{c}_{sk}F\frac{d\overline{\varphi}}{dx}\right)$$

(6.20)

Where the inverse of the solid/liquid friction coefficient can be defined as $d_h = 1/\alpha$, that is the mechanical permeability at zero electric potential gradient.

The molar flux of the i-th ion can be expressed as follows:

$$J_i = n\overline{c}_i(v_i - v_s) = n\overline{c}_i(v_i - v_w + v_w - v_s) = n\overline{c}_i(v_i - v_w) + q\overline{c}_i \qquad (6.21)$$

Substituting equation *(6.14b)* in equation *(6.21)*, we obtain:

$$J_i = q\overline{c}_i + \frac{n}{f_{wi}}\left(-\frac{d\overline{P}_i}{dx} - z_i\overline{c}_iF\frac{d\overline{\varphi}}{dx}\right) \qquad (6.21)$$

Since for dilute solution, the partial pressure of the ion species may be related to the ion concentration by means of the state equation of ideal gases:

$$\overline{P}_i = RT\overline{c}_i \quad i = 1,2,\dots,N \qquad (6.22)$$

where R is the universal gas constant (R = 8.314 J/(°K·mol)) and T is the absolute temperature.

Now, it is necessary to introduce the effective diffusion coefficient, which is a measure of the diffusion ability of the i-th ion inside a semi-permeable porous medium:

$$D_i^* = \frac{RT}{f_{wi}} \qquad (6.23)$$

Using equation *(6.21)*, *(6.22)* and *(6.23)* the Nernst-Planck Equations for a semipermeable porous medium is derived as:

$$J_i = q\bar{c}_i - nD_i^* \frac{d\bar{c}_i}{dx} - nz_i\bar{c}_i D_i^* \frac{F}{RT}\frac{d\bar{\varphi}}{dx} \tag{6.24}$$

The electric current density, I_e, carried by the mobile ions and by the fixed charge species is given by:

$$I_e = nF\left(\sum_{i=1}^N z_i\bar{c}_i v_i + \varpi\bar{c}_{sk}v_s\right) = nF\left(\sum_{i=1}^N z_i\bar{c}_i v_i - \sum_{i=1}^N z_i\bar{c}_i v_s\right) = \ldots$$

$$\ldots = nF\sum_{i=1}^N z_i\bar{c}_i\left(v_i - v_s\right) = F\sum_{i=1}^N z_i \cdot n\bar{c}_i\left(v_i - v_s\right) = F\sum_{i=1}^N z_i \cdot n\bar{c}_i\left(v_i - v_s\right) = \ldots \tag{6.25}$$

$$\ldots = F\sum_{i=1}^N z_i \cdot J_i$$

With the ion fluxes, J_i, given by equations *(6.24)*, the electric current density may be written as follows:

$$I_e = qF\sum_{i=1}^N z_i\bar{c}_i - nF\sum_{i=1}^N z_i D_i^* \frac{d\bar{c}_i}{dx} - n\frac{F^2}{RT}\left(\sum_{i=1}^N z_i^2\bar{c}_i D_i^*\right)\frac{d\bar{\varphi}}{dx} \tag{6.26}$$

The following quantities may be conveniently introduced:

(a) Equivalent electrical conductivity of i-th ion within the semi-permeable porous medium:

$$\bar{\kappa}_i = \frac{F^2}{RT}z_i^2\bar{c}_i D_i^* \tag{6.27}$$

(b) Equivalent electric conductivity of the solution within the semi-permeable porous medium:

$$\bar{\kappa} = \sum_{i=1}^N \bar{\kappa}_i = \frac{F^2}{RT}\sum_{i=1}^N z_i^2\bar{c}_i D_i^* \tag{6.28}$$

(c) The transference (6.or transport) number of the i-th ion within the semi-permeable porous medium:

$$\bar{t}_i = \frac{\bar{\kappa}_i}{\bar{\kappa}}$$

(6.29)

Using equations *(6.27)*, *(6.28)* and *(6.29)* in equation *(6.26)* an expression for the electric current, I_e, carried by the solution may be obtained as follows:

$$I_e = -\varpi \bar{c}_{sk} Fq - nF \sum_{i=1}^{N} z_i D_i^* \frac{d\bar{c}_i}{dx} - n\bar{\kappa} \frac{d\bar{\varphi}}{dx}$$

(6.30)

which may be rearranged to give the electric potential gradient:

$$\frac{d\bar{\varphi}}{dx} = -\varpi \bar{c}_{sk} \frac{F}{n\bar{\kappa}} q - \frac{I_e}{n\bar{\kappa}} - \frac{F}{\bar{\kappa}} \sum_{i=1}^{N} z_i D_i^* \frac{d\bar{c}_i}{dx}$$

(6.31)

Substituting equation (6.31) in equation (6.24) and, successively, using the definitions (6.27) and (6.29), the solute transport equation for a semi-permeable porous medium in the case of zero electric current can be obtained as follows:

$$J_i = q\bar{c}_i - nD_i^* \frac{d\bar{c}_i}{dx} + z_i \bar{c}_i D_i^* \frac{F^2}{RT} \frac{\varpi \bar{c}_{sk}}{\bar{\kappa}} q + nz_i \bar{c}_i D_i^* \frac{F^2}{RT} \frac{1}{\bar{\kappa}} \sum_{j=1}^{N} z_j D_j^* \frac{d\bar{c}_j}{dx} = ...$$

$$... = q\bar{c}_i \left(1 + \frac{\bar{t}_i}{z_i} \frac{\varpi \bar{c}_{sk}}{\bar{c}_i} \right) - nD_i^* \frac{d\bar{c}_i}{dx} + n\frac{\bar{t}_i}{z_i} \sum_{j=1}^{N} z_j D_j^* \frac{d\bar{c}_j}{dx}$$

(6.32)

6.2.4. Equations describing the mathematical model.

The simplified scheme, aimed at describing the problem exposed in the previous chapter (see Paragraph 6.2.1), consists of a "three ions + water solvent + charged solid" system.

To simplify matters,

1. Calcium cations are initially considered absent inside the natural Sodium bentonite layer, in which Sodium cations initially saturate the solid fixed charge;

2. The presence of Sodium cations is completely neglected outside the bentonite layer;

3. Chlorine anions do exist both inside and outside the bentonite layer.

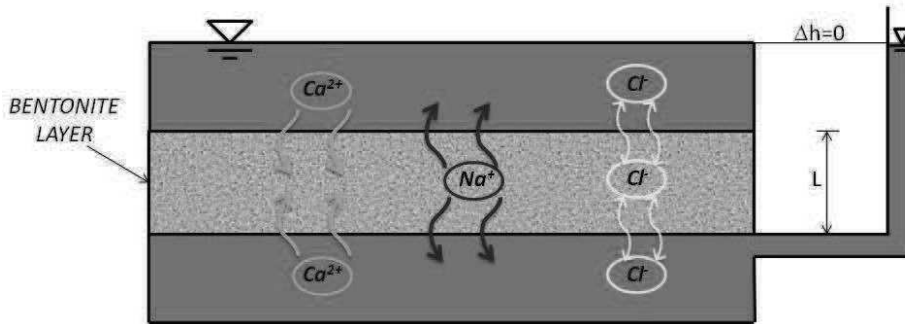A schematic representation of the system at time t > 0 is proposed in Figure 6.7.

Figure 6.7 – Schematic presentation of the studied system.

The developed mathematical model consists of two equations describing the simplified system in time and in space. Calcium and Chlorine concentrations (i.e. $\overline{c}_{Ca}$ and $\overline{c}_{Cl}$ respectively) are the adopted state variables and they are expressed as solute mass calculated inside an elementary soil volume. Calcium and Chlorine concentrations are dependent state variables that are function of time, t, and uni-dimensional space, x, which are independent variables.

The two equation system can be written as follows:

$$\begin{cases} \dfrac{\partial n\overline{c}_{Ca}}{\partial t} = -\dfrac{\partial J_{Ca}}{\partial x} \\[4mm] \dfrac{\partial n\overline{c}_{Cl}}{\partial t} = -\dfrac{\partial J_{Cl}}{\partial x} \end{cases} \qquad (6.33)$$

Where:

- n is the bentonite layer porosity in field conditions;

- $\overline{c}_{Ca}$ and $\overline{c}_{Cl}$ are respectively the Calcium and Chloride concentrations evaluated inside the bentonite layer,

- J_{Ca} and J_{Cl} are respectively the Calcium and Chloride flux, that can be expressed through the solute transport equation *(6.32)* for a semi-permeable porous medium, assuming that for very low hydraulic conductivity the volumetric flux of the solution is negligible ($q \approx 0$):

For Calcium:

$$J_{Ca} = -nD_{Ca}^* \frac{d\overline{c}_{Ca}}{dx} + n\frac{\overline{t}_{Ca}}{z_{Ca}}\left(z_{Ca}D_{Ca}^* \frac{d\overline{c}_{Ca}}{dx} + z_{Na}D_{Na}^* \frac{d\overline{c}_{Na}}{dx} + z_{Cl}D_{Cl}^* \frac{d\overline{c}_{Cl}}{dx} \right) = \dots$$

$$\dots = -nD_{Ca}^* \frac{d\overline{c}_{Ca}}{dx} + n\frac{\overline{t}_{Ca}}{2}\left(2D_{Ca}^* \frac{d\overline{c}_{Ca}}{dx} + D_{Na}^* \frac{d\overline{c}_{Na}}{dx} - D_{Cl}^* \frac{d\overline{c}_{Cl}}{dx} \right)$$

(6.34a)

For Chlorine:

$$J_{Cl} = -nD_{Cl}^* \frac{d\overline{c}_{Cl}}{dx} + n\frac{\overline{t}_{Cl}}{z_{Cl}}\left(z_{Ca}D_{Ca}^* \frac{d\overline{c}_{Ca}}{dx} + z_{Na}D_{Na}^* \frac{d\overline{c}_{Na}}{dx} + z_{Cl}D_{Cl}^* \frac{d\overline{c}_{Cl}}{dx} \right) = \dots$$

$$\dots = -nD_{Cl}^* \frac{d\overline{c}_{Cl}}{dx} - n\overline{t}_{Cl}\left(2D_{Ca}^* \frac{d\overline{c}_{Ca}}{dx} + D_{Na}^* \frac{d\overline{c}_{Na}}{dx} - D_{Cl}^* \frac{d\overline{c}_{Cl}}{dx} \right)$$

(6.34b)

Using the electro-neutrality condition, given by equation *(6.19)*, it is possible to express the derivative of Sodium concentration in space as a function of the derivative of Calcium and Chlorine concentrations in space:

$$2\overline{c}_{Ca} + \overline{c}_{Na} = \overline{c}_{sk} + \overline{c}_{Cl}$$
$$2\frac{d\overline{c}_{Ca}}{dx} + \frac{d\overline{c}_{Na}}{dx} = \frac{d\overline{c}_{sk}}{dx} + \frac{d\overline{c}_{Cl}}{dx}$$
$$\frac{d\overline{c}_{Na}}{dx} = \frac{d\overline{c}_{Cl}}{dx} - 2\frac{d\overline{c}_{Ca}}{dx}$$

(6.35)

Using equation *(6.35)* in equations *(6.34a)* and *(6.34b)* and rearranging, we obtain:

For Calcium:

$$J_{Ca} = -nD_{Ca}^* \frac{d\bar{c}_{Ca}}{dx} + n\frac{\bar{t}_{Ca}}{2}\left[2D_{Ca}^* \frac{d\bar{c}_{Ca}}{dx} + D_{Na}^* \left(\frac{d\bar{c}_{Cl}}{dx} - 2\frac{d\bar{c}_{Ca}}{dx} \right) - D_{Cl}^* \frac{d\bar{c}_{Cl}}{dx} \right] = ...$$

$$... = n\left[\left(-D_{Ca}^* + \bar{t}_{Ca}D_{Ca}^* - \bar{t}_{Ca}D_{Na}^* \right)\frac{d\bar{c}_{Ca}}{dx} + \left(\bar{t}_{Ca}\frac{D_{Na}^*}{2} - \bar{t}_{Ca}\frac{D_{Cl}^*}{2} \right)\frac{d\bar{c}_{Cl}}{dx} \right] = ...$$

$$J_{Ca} = n\left[D_{Ca}^*\left(\bar{t}_{Ca} - \bar{t}_{Ca}\frac{D_{Na}^*}{D_{Ca}^*} - 1 \right)\frac{d\bar{c}_{Ca}}{dx} + D_{Cl}^*\frac{\bar{t}_{Ca}}{2}\left(\frac{D_{Na}^*}{D_{Cl}^*} - 1 \right)\frac{d\bar{c}_{Cl}}{dx} \right]$$

(6.36a)

For Chlorine:

$$J_{Cl} = -nD_{Cl}^* \frac{d\bar{c}_{Ca}}{dx} - n\bar{t}_{Cl}\left[2D_{Ca}^* \frac{d\bar{c}_{Ca}}{dx} + D_{Na}^* \left(\frac{d\bar{c}_{Cl}}{dx} - 2\frac{d\bar{c}_{Ca}}{dx} \right) - D_{Cl}^* \frac{d\bar{c}_{Cl}}{dx} \right] = ...$$

$$... = n\left[\left(-2\bar{t}_{Cl}D_{Ca}^* + 2\bar{t}_{Cl}D_{Na}^* \right)\frac{d\bar{c}_{Ca}}{dx} + \left(-D_{Cl}^* + \bar{t}_{Cl}D_{Na}^* + \bar{t}_{Cl}D_{Cl}^* \right)\frac{d\bar{c}_{Cl}}{dx} \right] = ...$$

$$J_{Cl} = n\left[2\bar{t}_{Cl}D_{Ca}^*\left(\frac{D_{Na}^*}{D_{Ca}^*} - 1 \right)\frac{d\bar{c}_{Ca}}{dx} + D_{Cl}^*\left(\bar{t}_{Cl} - \bar{t}_{Cl}\frac{D_{Na}^*}{D_{Cl}^*} - 1 \right)\frac{d\bar{c}_{Cl}}{dx} \right]$$

(6.36b)

Equations *(6.36a)* and *(6.36b)* can be written in matrix as follows:

$$\begin{bmatrix} J_{Ca} \\ J_{Cl} \end{bmatrix} = \begin{bmatrix} D_{11} & D_{12} \\ D_{21} & D_{22} \end{bmatrix} \cdot \begin{bmatrix} \dfrac{d\bar{c}_{Ca}}{dx} \\ \dfrac{d\bar{c}_{Cl}}{dx} \end{bmatrix}$$

(6.37)

Where:

$$
\begin{cases}
D_{11} = D_{Ca}^* \left(\bar{t}_{Ca} - \bar{t}_{Ca} \dfrac{D_{Na}^*}{D_{Ca}^*} - 1 \right) \\[4mm]
D_{12} = D_{Cl}^* \dfrac{\bar{t}_{Ca}}{2} \left(\dfrac{D_{Na}^*}{D_{Cl}^*} - 1 \right) \\[4mm]
D_{21} = 2\bar{t}_{Cl} D_{Ca}^* \left(\dfrac{D_{Na}^*}{D_{Ca}^*} - 1 \right) \\[4mm]
D_{22} = D_{Cl}^* \left(\bar{t}_{Cl} - \bar{t}_{Cl} \dfrac{D_{Na}^*}{D_{Cl}^*} - 1 \right)
\end{cases}
\qquad (6.38)
$$

Once known the dependent state variables $\bar{c}_{Ca}$ and $\bar{c}_{Cl}$, the Sodium concentration can be calculated, for each value of t and x, using equation *(6.19)*:

$$
\bar{c}_{Na} = \bar{c}_{sk} + \bar{c}_{Cl} - 2\bar{c}_{Ca} \qquad (6.39)
$$

6.3   SOLUTION METHOD

This paragraph is aimed at developing a numerical solution of the mathematical problem. The process consists of the definition of a consistent and well formulated mathematical problem by the selection of necessary initial and boundary conditions aimed to resolve the equation system derived in the previous paragraph, which describes the studied phenomenon.

The mathematical model is a partial differential equation system. It can be defined 'consistent' because the equation number, which is 2 as reported in equation (6.33), is equal to the independent unknown number, which is 2 again: $\bar{c}_{Ca}$ and $\bar{c}_{Cl}$, because the Sodium concentration can be calculated, once known Calcium and Chlorine concentrations, using equation (6.39).

A 'well formulated' problem is associated to a certain number of initial and boundary conditions that are enough to find its solution. Since in the studied mathematical model, both the time derivative and the spatial derivative appear, it is necessary to assign both the initial and the boundary conditions.

6.3.1. Dimensionless equations.

With the aim to formulate the mathematical problem, two reasons make necessary to write dimensionless equations: first of all, when a physical phenomenon is described the variable behaviour may be more significant if compared with a reference value; moreover, when numerical methods need to be applied, dimensionless equations bring to important computational advantages (since the variation of several orders of magnitude, in time or in space, may give troubles to the calculator).

The following dimensionless variables are defined:

$$\left\{ \begin{array}{ll} \upsilon_1 = \dfrac{\overline{c}_{Ca}}{\overline{c}_r} & \text{(6.40a)} \\[2em] \upsilon_2 = \dfrac{\overline{c}_{Cl}}{\overline{c}_r} & \text{(6.40b)} \\[2em] X = \dfrac{x}{L} & \text{(6.40c)} \\[2em] T = \dfrac{t}{t_0} = \dfrac{t \cdot D_{Ca}^*}{L^2} & \text{(6.40d)} \end{array} \right.$$

Where:

- υ_1 and υ_2 are respectively the dimensionless Calcium and Chlorine concentration

(by analogy, the dimensionless Sodium concentration can be defined as: $\upsilon_3 = \dfrac{\overline{c}_{Na}}{\overline{c}_r}$);

- $\overline{c}_r$ is the reference concentration that will be afterwards defined;

- X is the dimensionless spatial variable;

- L is the bentonite layer thickness;

- T is the dimensionless time variable;

- t_0, defined as in equation (6.40d), is the diffusive time factor.

Under the hypothesis of uncompressible porous medium (n = constant), the equation system (6.33) can be simplified as follows:

$$\begin{cases} \dfrac{d\overline{c}_{Ca}}{dt} = -\dfrac{d}{dx}\left(D_{11}\dfrac{d\overline{c}_{Ca}}{dx} + D_{12}\dfrac{d\overline{c}_{Cl}}{dx} \right) \\[3mm] \dfrac{d\overline{c}_{Cl}}{dt} = -\dfrac{d}{dx}\left(D_{21}\dfrac{d\overline{c}_{Ca}}{dx} + D_{22}\dfrac{d\overline{c}_{Cl}}{dx} \right) \end{cases} \qquad (6.41)$$

Using the dimensionless variables in equations (6.40a), (6.40b), (6.40c) and (6.40d), the equation system (6.41) can be expressed in the following dimensionless form:

$$\begin{cases} \overline{c}_r \dfrac{D_{Ca}^*}{L^2}\dfrac{d\upsilon_1}{dT} = -\dfrac{1}{L}\dfrac{d}{dX}\left(\dfrac{D_{11}\overline{c}_r}{L}\dfrac{d\upsilon_1}{dX} + \dfrac{D_{12}\overline{c}_r}{L}\dfrac{d\upsilon_2}{dX} \right) \\[3mm] \overline{c}_r \dfrac{D_{Ca}^*}{L^2}\dfrac{d\upsilon_2}{dT} = -\dfrac{1}{L}\dfrac{d}{dX}\left(\dfrac{D_{21}\overline{c}_r}{L}\dfrac{d\upsilon_1}{dX} + \dfrac{D_{22}\overline{c}_r}{L}\dfrac{d\upsilon_2}{dX} \right) \end{cases}$$

That becomes by simplifying:

$$\begin{cases} \dfrac{d\upsilon_1}{dT} = -\dfrac{1}{D_{Ca}^*}\dfrac{d}{dX}\left(D_{11}\dfrac{d\upsilon_1}{dX} + D_{12}\dfrac{d\upsilon_2}{dX} \right) \\[3mm] \dfrac{d\upsilon_2}{dT} = -\dfrac{1}{D_{Ca}^*}\dfrac{d}{dX}\left(D_{21}\dfrac{d\upsilon_1}{dX} + D_{22}\dfrac{d\upsilon_2}{dX} \right) \end{cases} \qquad (6.42)$$

6.3.2. Finite-difference method solution.

The dimensionless equation system (6.42) is a non-linear parabolic system. Both equations are non-linear because the coefficients $D_{11}, \ldots D_{22}$ depend on Calcium and Chloride concentration through the terms $\overline{t}_{Ca}$ and $\overline{t}_{Cl}$ (see equation (6.29)). It is a typical diffusion-type problem that can be discretized using the simple explicit method, expressed as follows (Özisik, 1993; Bellomo and Preziosi, 1995):

$$\dfrac{dT}{dt} = \dfrac{d}{dx}\left(k(T)\dfrac{dT}{dx} \right) \quad \Rightarrow \quad \dfrac{T_i^{n+1} - T_i^n}{\Delta t} = k_{i-\frac{1}{2}}\dfrac{T_{i-1}^n - T_i^n}{(\Delta x)^2} + k_{i+\frac{1}{2}}\dfrac{T_{i+1}^n - T_i^n}{(\Delta x)^2}$$

$$(6.43)$$

The dimensionless equation system described in equation (6.42) can be discretized, using finite differences centred in space and the forward Euler method in time, as follows:

$$
\begin{cases}
\dfrac{\upsilon_{1,i}^{n+1} - \upsilon_{1,i}^{n}}{\Delta T} = \left[D_{11,i-\frac{1}{2}}^{n} \dfrac{\upsilon_{1,i-1}^{n} - \upsilon_{1,i}^{n}}{(\Delta X)^2} + D_{11,i+\frac{1}{2}}^{n} \dfrac{\upsilon_{1,i+1}^{n} - \upsilon_{1,i}^{n}}{(\Delta X)^2} + D_{12,i-\frac{1}{2}}^{n} \dfrac{\upsilon_{2,i-1}^{n} - \upsilon_{2,i}^{n}}{(\Delta X)^2} + D_{12,i+\frac{1}{2}}^{n} \dfrac{\upsilon_{2,i+1}^{n} - \upsilon_{2,i}^{n}}{(\Delta X)^2} \right] \\[4mm]
\dfrac{\upsilon_{2,i}^{n+1} - \upsilon_{2,i}^{n}}{\Delta T} = \left[D_{21,i-\frac{1}{2}}^{n} \dfrac{\upsilon_{1,i-1}^{n} - \upsilon_{1,i}^{n}}{(\Delta X)^2} + D_{21,i+\frac{1}{2}}^{n} \dfrac{\upsilon_{1,i+1}^{n} - \upsilon_{1,i}^{n}}{(\Delta X)^2} + D_{22,i-\frac{1}{2}}^{n} \dfrac{\upsilon_{2,i-1}^{n} - \upsilon_{2,i}^{n}}{(\Delta X)^2} + D_{22,i+\frac{1}{2}}^{n} \dfrac{\upsilon_{2,i+1}^{n} - \upsilon_{2,i}^{n}}{(\Delta X)^2} \right]
\end{cases}
$$

$$(6.44)$$

Where:

$$
\begin{cases}
D_{11,i\pm\frac{1}{2}}^{n} = \overline{t}_{Ca,i\pm\frac{1}{2}}^{n} - \overline{t}_{Ca,i\pm\frac{1}{2}}^{n} \cdot \dfrac{D_{Na}^{*}}{D_{Ca}^{*}} - 1 & (6.45a) \\[5mm]
D_{12,i\pm\frac{1}{2}}^{n} = \dfrac{\overline{t}_{Ca,i\pm\frac{1}{2}}^{n}}{2} \cdot \dfrac{D_{Cl}^{*}}{D_{Ca}^{*}} \left(\dfrac{D_{Na}^{*}}{D_{Cl}^{*}} - 1 \right) & (6.45b) \\[5mm]
D_{21,i\pm\frac{1}{2}}^{n} = 2 \cdot \overline{t}_{Cl,i\pm\frac{1}{2}}^{n} \left(\dfrac{D_{Na}^{*}}{D_{Ca}^{*}} - 1 \right) & (6.45c) \\[5mm]
D_{22,i\pm\frac{1}{2}}^{n} = \dfrac{D_{Cl}^{*}}{D_{Ca}^{*}} \left(\overline{t}_{Cl,i\pm\frac{1}{2}}^{n} - \overline{t}_{Cl,i\pm\frac{1}{2}}^{n} \cdot \dfrac{D_{Na}^{*}}{D_{Cl}^{*}} - 1 \right) & (6.45d)
\end{cases}
$$

And: <u>For Calcium:</u>

$$t_{Ca,i\pm\frac{1}{2}}^{n} = \frac{\overline{\kappa}_{Ca}}{\overline{\kappa}} = \frac{4D_{Ca}^{*} \cdot \overline{C}_{Ca,i\pm\frac{1}{2}}^{n}}{D_{Na}^{*} \cdot \overline{C}_{Na,i\pm\frac{1}{2}}^{n} + 4D_{Ca}^{*} \cdot \overline{C}_{Ca,i\pm\frac{1}{2}}^{n} + D_{Cl}^{*} \cdot \overline{C}_{Cl,i\pm\frac{1}{2}}^{n}} = ...$$

$$... = \frac{4D_{Ca}^{*} \cdot \overline{C}_{Ca,i\pm\frac{1}{2}}^{n}}{D_{Na}^{*} \cdot \left(\overline{C}_{X} + \overline{C}_{Cl,i\pm\frac{1}{2}}^{n} - 2\overline{C}_{Ca,i\pm\frac{1}{2}}^{n} \right) + 4D_{Ca}^{*} \cdot \overline{C}_{Ca,i\pm\frac{1}{2}}^{n} + D_{Cl}^{*} \cdot \overline{C}_{Cl,i\pm\frac{1}{2}}^{n}} = ...$$

$$... = \frac{4D_{Ca}^{*} \cdot \overline{C}_{Ca,i\pm\frac{1}{2}}^{n}}{D_{Na}^{*} \cdot \overline{C}_{X} + \left(D_{Na}^{*} + D_{Cl}^{*} \right) \cdot \overline{C}_{Cl,i\pm\frac{1}{2}}^{n} + \left(4D_{Ca}^{*} - 2D_{Na}^{*} \right) \cdot \overline{C}_{Ca,i\pm\frac{1}{2}}^{n}} = ...$$

$$... = \frac{4D_{Ca}^{*} \cdot \overline{C}_{r} \upsilon_{1,i\pm\frac{1}{2}}^{n}}{\overline{C}_{r} \left[D_{Na}^{*} \cdot \frac{\overline{C}_{X}}{\overline{C}_{r}} + \left(D_{Na}^{*} + D_{Cl}^{*} \right) \cdot \upsilon_{2,i\pm\frac{1}{2}}^{n} + \left(4D_{Ca}^{*} - 2D_{Na}^{*} \right) \cdot \upsilon_{1,i\pm\frac{1}{2}}^{n} \right]} = ...$$

$$\Rightarrow \qquad t_{Ca,i\pm\frac{1}{2}}^{n} = \frac{4D_{Ca}^{*} \cdot \upsilon_{1,i\pm\frac{1}{2}}^{n}}{D_{Na}^{*} \cdot \frac{\overline{C}_{X}}{\overline{C}_{r}} + \left(D_{Na}^{*} + D_{Cl}^{*} \right) \cdot \upsilon_{2,i\pm\frac{1}{2}}^{n} + \left(4D_{Ca}^{*} - 2D_{Na}^{*} \right) \cdot \upsilon_{1,i\pm\frac{1}{2}}^{n}}$$

$$(6.46)$$

For Chlorine:

$$t_{Cl,i\pm\frac{1}{2}}^{n} = \frac{\overline{\kappa}_{Cl}}{\overline{\kappa}} = \frac{D_{Cl}^{*}\cdot\overline{C}_{Cl,i\pm\frac{1}{2}}^{n}}{D_{Na}^{*}\cdot\overline{C}_{X}+\left(D_{Na}^{*}+D_{Cl}^{*}\right)\cdot\overline{C}_{Cl,i\pm\frac{1}{2}}^{n}+\left(4D_{Ca}^{*}-2D_{Na}^{*}\right)\cdot\overline{C}_{Ca,i\pm\frac{1}{2}}^{n}} = ...$$

$$... = \frac{D_{Cl}^{*}\cdot\overline{C}_{r}\upsilon_{2,i\pm\frac{1}{2}}^{n}}{\overline{C}_{r}\left[D_{Na}^{*}\cdot\dfrac{\overline{C}_{X}}{\overline{C}_{r}}+\left(D_{Na}^{*}+D_{Cl}^{*}\right)\cdot\upsilon_{2,i\pm\frac{1}{2}}^{n}+\left(4D_{Ca}^{*}-2D_{Na}^{*}\right)\cdot\upsilon_{1,i\pm\frac{1}{2}}^{n}\right]} = ...$$

$$\Rightarrow \qquad t_{Ca,i\pm\frac{1}{2}}^{n} = \frac{D_{Cl}^{*}\cdot\upsilon_{2,i\pm\frac{1}{2}}^{n}}{D_{Na}^{*}\cdot\dfrac{\overline{C}_{X}}{\overline{C}_{r}}+\left(D_{Na}^{*}+D_{Cl}^{*}\right)\cdot\upsilon_{2,i\pm\frac{1}{2}}^{n}+\left(4D_{Ca}^{*}-2D_{Na}^{*}\right)\cdot\upsilon_{1,i\pm\frac{1}{2}}^{n}}$$

$$(6.47)$$

The finite difference conceptual scheme is reported in Figure 6.8. It is a mono-dimensional model divided, in space, into nx nodes and, in time, into nt time steps.

Figure 6.8 – Model FDM conceptual scheme.

6.3.3. Initial and boundary conditions – Study of the partition mechanism in the pore solution.

Since the mathematical model presents both the spatial and the time derivatives, it is necessary to assign both the initial conditions and the conditions at the boundaries.

The initial and boundary conditions are assigned to the upper and lower reservoirs that contain the bentonite layer, as already reported in the schematic presentation in Figure 6.3.

For plainness, the thermodynamic variables of the model are over-signed (e.g. $\overline{c}_i$) because represent the values that can be virtually measured inside the porous medium. These values are influenced by the presence of the solid charge and, consequently, by the presence of the fixed charge concentration ($\overline{c}_{sk}$).

Contrariwise the variables representing the reservoir characteristics outside the porous medium are not over-signed.

Moreover the values of the thermodynamic variables are the same inside the two reservoirs.

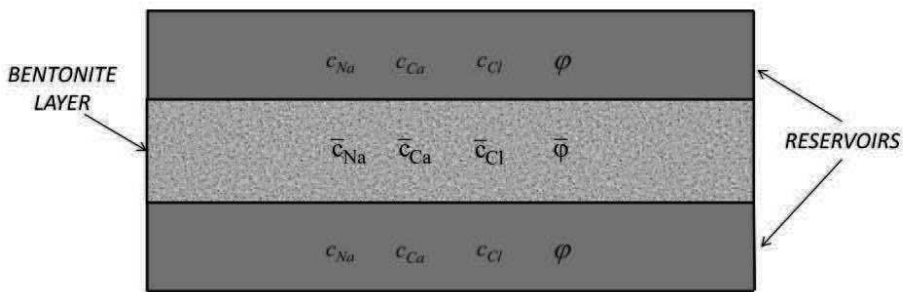In Figure6.9 these simple conventions are reported.

Figure 6.9 – Schematic presentation of the studied system.

In a charged porous medium (i.e. the bentonite layer in the studied model) the concentration of the i-th ion in the solution contained inside the pore ($\overline{c}_i$) can be related to the concentration of the i-th ion in the 'virtual' solution (c_i), which is

contained inside the two 'virtual' reservoirs and is in thermodynamic equilibrium with the porous medium, by a simple relation, such as:

$$\bar{c}_i = \Gamma_i \cdot c_i \qquad (6.48)$$

where Γ_i is the partition coefficient of the i-th ion that characterized the relevance of partition effect.

With the aim to assign initial and boundary conditions to the solution contained inside the external reservoirs, the ion partition mechanism in the pore solution has to be studied.

The partition coefficient of the i-th ion may be expressed using Donnan's model (Dominijanni, 2005):

$$\Gamma_i = \exp\left(-\frac{z_i F \left(\bar{\varphi} - \varphi\right)}{RT}\right) \qquad (6.49)$$

Where F is the Faraday constant.

Since the solid phase of bentonite is, generally, negatively charged, the cations result attracted by the porous medium, while the anion are repelled. Thereby the cation partition coefficient is larger than 1, whereas the anion partition coefficient is smaller than 1.

6.3.3.1 Initial conditions.

The initial conditions are imposed by assigning an initial and instantaneous Sodium Chloride concentration inside the external reservoirs (i.e. $c_{0,NaCl}$). Such a concentration determines the saturation of bentonite exchange complex and the presence of soluble Sodium inside the voids.

Moreover, this condition implies the initial absence of Calcium in the pore solution contained inside the porous medium.

In the case of NaCl, the molecules are dissociated as follows:

$$NaCl \rightarrow Na^+ + Cl^-$$

$$c_{0,NaCl} = c_{Na^+} = c_{Cl^-}$$

As shown in the previous paragraph, the macroscopic electroneutrality in the pore is described by the equation (6.19), which, in the case of single salt (NaCl), becomes:

$$\overline{c}_{Na^+} - \overline{c}_{Cl^-} - \overline{c}_{sk} = 0 \tag{6.50}$$

If the only considered partition mechanism is that due to the electric potential of solid phase, then from equation (6.49), a relation between the partition coefficient of counter-ion (Γ_1) and the one of the co-ion (Γ_2) can be derived:

$$\Gamma_1 = \Gamma_2^{\frac{v_2}{v_1}} = \Gamma_2^{\frac{|z_1|}{|z_2|}} \tag{6.51}$$

In the case of NaCl we obtain:

$$\Gamma_{Na^+} = \Gamma_{Cl^-}^{-1} \tag{6.52}$$

where:

$$\begin{cases} \Gamma_{Na^+} = \dfrac{\overline{c}_{Na^+}}{c_{Na^+}} = \dfrac{\overline{c}_{Na^+}}{c_{0,NaCl}} \\[3mm] \Gamma_{Cl^-} = \dfrac{\overline{c}_{Cl^-}}{c_{Cl^-}} = \dfrac{\overline{c}_{Cl^-}}{c_{0,NaCl}} \end{cases}$$

Using equation (6.50) and (6.52), it is possible to derive the Chlorine partition coefficient, as a function of the relative fixed charge concentration ($\dfrac{\overline{c}_{sk}}{c_{0,NaCl}}$), as follows:

$$\frac{1}{\Gamma_{Cl^-}} - \Gamma_{Cl^-} - \frac{\overline{c}_{sk}}{c_{0,NaCl}} = 0$$

$$1 - \Gamma_{Cl^-}^2 - \frac{\overline{c}_x}{c_{0,NaCl}} \Gamma_{Cl^-} = 0$$

$$\Gamma_{Cl^-} = -\frac{\overline{c}_{sk}}{2c_{0,NaCl}} + \sqrt{\left(\frac{\overline{c}_{sk}}{2c_{0,NaCl}}\right)^2 + 1} \tag{6.53}$$

Once solved equation (6.53), the Sodium partition coefficient can be easily calculated using equation (6.52).

Finally, the mathematical model initial conditions are defined as follows:

$$\text{For } t = 0, \forall x \quad \Rightarrow \quad \begin{cases} \bar{c}_{Ca}^0 = 0 \\ \bar{c}_{Cl}^0 = \Gamma_{Cl} \cdot c_{0,NaCl}^0 \\ \bar{c}_{Na}^0 = \Gamma_{Na} \cdot c_{0,NaCl}^0 \end{cases} \tag{6.54}$$
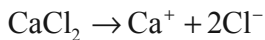
And, consequently, the dimensionless initial conditions are:

$$\text{For } t = 0, \forall x \quad \Rightarrow \quad \begin{cases} v_1^0 = 0 \\ v_2^0 = \dfrac{\Gamma_{Cl} \cdot c_{0,NaCl}^0}{\bar{c}_r} \\ v_3^0 = \dfrac{\Gamma_{Na} \cdot c_{0,NaCl}^0}{\bar{c}_r} \end{cases} \tag{6.55}$$

Where $\bar{c}_r$ is the reference concentration used to define the dimensionless variables in equations (6.40a,b).

6.3.3.2 Boundary conditions.

The boundary conditions are imposed by assigning a constant Calcium Chloride concentration inside the external reservoirs (i.e. c_0). Such a concentration determines the migration of Calcium from outside to inside the model boundaries. The Calcium concentration in the first (i.e. '1' in Figure 4.1) and last (i.e. 'nx' in Figure 4.1) nodes of the model results constant in time and it is given by equation (6.48). In the particular case of $CaCl_2$, the molecule is dissociated in:

$$CaCl_2 \rightarrow Ca^+ + 2Cl^-$$

$$c_0 = c_{Ca^{2+}} = \frac{c_{Cl^-}}{2}$$

The equations (6.19) and (6.51) become respectively:

$$2\overline{c}_{Ca^{2+}} - \overline{c}_{Cl^-} - \overline{c}_{sk} = 0 \tag{6.56}$$

$$\Gamma_{Ca^{2+}} = \Gamma_{Cl^-}^{-2} \tag{6.57}$$

where:
$$\begin{cases} \Gamma_{Ca^{2+}} = \dfrac{\overline{c}_{Ca^{2+}}}{c_{Ca^{2+}}} = \dfrac{\overline{c}_{Ca^{2+}}}{c_0} \\[3mm] \Gamma_{Cl^-} = \dfrac{\overline{c}_{Cl^-}}{c_{Cl^-}} = \dfrac{\overline{c}_{Cl^-}}{2c_0} \end{cases}$$

Using equation (6.56) and (6.57), the anion partition coefficient as a function of the relative fixed charge concentration for a (6.2:1) electrolyte is deduced by the following procedure:

$$2c_0\Gamma_{Cl^-}^{-2} - \Gamma_{Cl^-}2c_0 - \overline{c}_{sk} = 0$$

$$\left(\Gamma_{Cl^-}\right)^{-2} - \Gamma_{Cl^-} - \frac{\overline{c}_{sk}}{2c_0} = 0$$

$$1 - \Gamma_{Cl^-}^{3} - \frac{\overline{c}_{sk}}{2c_0}\Gamma_{Cl^-}^{2} = 0$$

$$\Gamma_{Cl^-} = \frac{2}{3\tau\left(\dfrac{\overline{c}_{sk}}{2c_0}\right)}\left(\frac{\overline{c}_{sk}}{2c_0}\right)^2 - \frac{1}{3}\left(\frac{\overline{c}_{sk}}{2c_0}\right) + \frac{1}{6}\tau\left(\frac{\overline{c}_{sk}}{2c_0}\right) \tag{6.58}$$

Where: $\tau(\alpha) = \left[108 - 8\alpha^3 + 12\left(81 - 12\alpha^3\right)^{\frac{1}{2}}\right]^{\frac{1}{3}}$

Once solved equation (6.58), the Calcium partition coefficient can be easily calculated using equation (6.57).

Concluding, the mathematical model boundary conditions are defined as follows:

For $x = 1$ and $x = nx$, $\forall t$ $\Rightarrow$

$$\begin{cases} \overline{c}_{Ca,1} = \overline{c}_{Ca,nx} = \Gamma_{Ca} \cdot c_0 \\ \overline{c}_{Cl,1} = \overline{c}_{Cl,nx} = 2 \cdot \Gamma_{Cl} \cdot c_0 \end{cases}$$

(6.59)

And, consequently, the dimensionless boundary conditions are:

For $x = 1$ and $x = nx$, $\forall t$ $\Rightarrow$

$$\begin{cases} \upsilon_{1,1} = \upsilon_{1,nx} = \dfrac{\Gamma_{Ca} \cdot c_0}{\overline{c}_r} = 1 \\ \upsilon_{2,1} = \upsilon_{2,nx} = \dfrac{2\Gamma_{Cl} \cdot c_0}{\overline{c}_r} \end{cases}$$

(6.60)

Where $\overline{c}_r$ is the reference concentration used to define the dimensionless variables in equations (6.40a,b) that is constant and defined as: $\overline{c}_r = \Gamma_{Ca} \cdot c_0$.

6.4   MATLAB® IMPLEMENTATION

The solution method described in the previous paragraph is implemented in MATLAB®. The programme script is reported in this paragraph.

```
%input data:

%BENTONITE.
L=0.01; %[m] - bentonite layer thickness
n=0.81; %[-] - bentonite layer porosity
tau=0.31; %[-] - bentonite layer tortuosity coefficient
Cx0=0.09; %[mol/L] - montmorillonite fixed charge coefficient referred to the
solid skeleton

%SOLUTION.
D0Ca=7.92*10^(-10); %[m^2/s] - calcium free solution diffusion coefficient
D0Na=13.3*10^(-10); %[m^2/s] - sodium free solution diffusion coefficient
D0Cl=20.3*10^(-10); %[m^2/s] - chlorine free solution diffusion coefficient
C0=0.02; %[mol/L] - natural calcium cloride concentration in common soil
```

```
%OTHER.
R=8.314; %[N*m/(mol*K)] - universal gas costant
T=273+20; %[K] - absolute temperature



%calculated parameters:


eb=n/(1-n); %[-] - bentonite layer void ratio
Cx=Cx0/eb; %[mol/L] - montmorillonite fixed charge coefficient referred to
the pore space
DCa=D0Ca*tau; %[m^2/s] - calcium effective diffusion coefficient
DNa=D0Na*tau; %[m^2/s] - sodium effective diffusion coefficient
DCl=D0Cl*tau; %[m^2/s] - chlorine effective diffusion coefficient


% differential equations solution:

%FDM PARAMETERS.
nx=41; %[-] - node number
nxx=nx-1;
dx=1/nxx; %[-] - finite distance between two subsequent nodes
x=[0:dx:1]; %[-] - spatial coordinate


tannifin=10/365; %[anni]
t0=L^2/DCa; % [s] - reference time
tfin=tannifin*(60*60*24*365)/t0; % [-] - dimensionless final time
dt=0.0001; % [-] - time discretisation
nt=tfin/dt; % [-] - number of time step


%INITIAL CONDITIONS.


C0NaCl=0.05; %[mol/L] - initial external sodium chloride concentration
GCl0=-Cx/(2*C0NaCl)+sqrt((Cx/(2*C0NaCl))^2+1);  %[-] - chlorine  partition
coefficient
GNa0=GCl0^(-1); %[-] - sodium partition coefficient
CNa0=GNa0*C0NaCl;  %[mol/L]
CCl0=GCl0*C0NaCl;  %[mol/L]


%BOUNDARY CONDITIONS.


alfa=Cx/(2*C0);
aux=(108-(8*(alfa^3))+12*sqrt(81-(12*(alfa^3))))^(1/3);
GCl=real((2/(3*aux))*(alfa^2)-(1/3)*alfa+(1/6)*aux);    %[-]   -   chlorine
partition coefficient
GCa=GCl^(-2); %[-] - calcium partition coefficient
```

```
CCl=GCl*C0*2; %[mol/L]
CCa=GCa*C0; %[mol/L]
Cr=CCa; %[mol/L] reference concentration
u1(1)=1;
u2(1)=CCl/Cr;
u1(nx)=1;
u2(nx)=CCl/Cr;

t=0;
for ix=2:nxx
    u1(ix)=0;
    u2(ix)=CCl0/Cr;
end

for ix=1:nx
    u3(ix)=(CNa0)/Cr;
end

%CALCULATIONS.

snapt1(1)=u1(nxx/2);
snapt2(1)=u2(nxx/2);
snapt3(1)=u3(nxx/2);
snaptCx(1)=Cx;
t(1)=0;
snap3D1(1,:)=u1;
snap3D2(1,:)=u2;
snap3D3(1,:)=u3;
tt3D(1)=0;

for it=1:nt
    u1old=u1;
    u2old=u2;
    for ixbis=1:nxx
        u1oldbis(ixbis)=(u1old(ixbis)+u1old(ixbis+1))/2;
        u2oldbis(ixbis)=(u2old(ixbis)+u2old(ixbis+1))/2;

tCa(ixbis)=4*DCa*u1oldbis(ixbis)/(DNa*Cx/Cr+(DNa+DCl)*u2oldbis(ixbis)+(4*DCa-
2*DNa)*u1oldbis(ixbis));

tCl(ixbis)=DCl*u2oldbis(ixbis)/(DNa*Cx/Cr+(DNa+DCl)*u2oldbis(ixbis)+(4*DCa-
2*DNa)*u1oldbis(ixbis));
        D11(ixbis)=-(tCa(ixbis)-tCa(ixbis)*DNa/DCa-1);
        D12(ixbis)=-(tCa(ixbis)/2*DCl/DCa*(DNa/DCl-1));
```

```matlab
        D21(ixbis)=-(2*tCl(ixbis)*(DNa/DCa-1));
        D22(ixbis)=-(DCl/DCa*(tCl(ixbis)-tCl(ixbis)*DNa/DCl-1));
    end


    for ix=2:nxx
        d2bu1(ix)=(u1old(ix-1)-u1old(ix))/(dx^2);
        d2bu2(ix)=(u2old(ix-1)-u2old(ix))/(dx^2);
        d2fu1(ix)=(u1old(ix+1)-u1old(ix))/(dx^2);
        d2fu2(ix)=(u2old(ix+1)-u2old(ix))/(dx^2);
        u1(ix)=u1old(ix)+(D11(ix-1)*d2bu1(ix)+D11(ix)*d2fu1(ix)+D12(ix-
1)*d2bu2(ix)+D12(ix)*d2fu2(ix))*dt;
        u2(ix)=u2old(ix)+(D21(ix-1)*d2bu1(ix)+D21(ix)*d2fu1(ix)+D22(ix-
1)*d2bu2(ix)+D22(ix)*d2fu2(ix))*dt;
    end
    for ix=1:nx
        u3(ix)=Cx/Cr+u2(ix)-2*u1(ix);
    end
    t=it*dt;
    snapt1(it+1)=u1(nxx/2);
    snapt2(it+1)=u2(nxx/2);
    snapt3(it+1)=u3(nxx/2);
    snaptCx(it+1)=Cx;
    snap3D1(it+1,:)=u1;
    snap3D2(it+1,:)=u2;
    snap3D3(it+1,:)=u3;
    tt(it+1)=t;
    tt3D=[tt3D; t];
end

ttdays=tt*t0/(60*60*24);
tt3Ddays=tt3D*t0/(60*60*24);

%FIGURES.

figure(1);
plot(x,u1,x,u2,x,u3);
legend('c_C_a/c_C_a_0','c_C_l/c_C_a_0','c_N_a/c_C_a_0');
xlabel('X=x/L');ylabel('c/c_C_a_0');
figure(2);
plot(ttdays,snapt1*Cr,ttdays,snapt2*Cr,ttdays,snapt3*Cr,ttdays,snaptCx);
legend('c_C_a','c_C_l','c_N_a','c_s_k');
xlabel('Time, t [d]');ylabel('Ion concentration, c_i [mol/L]');
figure(3);
clf
```

```
mesh(x,tt3Ddays,snap3D1*Cr), grid on
xlabel('Relative distance inside the bentonite layer, x [-]')
ylabel('Time, t [d]')
zlabel('Calcium concentration, c_C_a [mol/L]')
figure(4);
clf
mesh(x,tt3Ddays,snap3D2*Cr), grid on
xlabel('Relative distance inside the bentonite layer, x [-]')
ylabel('Time, t [d]')
zlabel('Chlorine concentration, c_C_l [mol/L]')
figure(5);
clf
mesh(x,tt3Ddays,snap3D3*Cr), grid on
xlabel('Relative distance inside the bentonite layer, x [-]')
ylabel('Time, t [d]')
zlabel('Sodium concentration, c_N_a [mol/L]')
```

```
clear all
```

```
%input data:

%BENTONITE.
L=0.02; %[m] - bentonite layer thickness
n=0.81; %[-] - bentonite layer porosity
tau=0.31; %[-] - bentonite layer tortuosity coefficient
Cx0=0.09; %[mol/L] - montmorillonite fixed charge coefficient referred to the
solid skeleton

%SOLUTION.
D0Ca=7.92*10^(-10); %[m^2/s] - calcium free solution diffusion coefficient
D0Na=13.3*10^(-10); %[m^2/s] - sodium free solution diffusion coefficient
D0Cl=20.3*10^(-10); %[m^2/s] - chlorine free solution diffusion coefficient
C0=0.02; %[mol/L] - natural calcium cloride concentration in common soil

%OTHER.
R=8.314; %[N*m/(mol*K)] - universal gas costant
T=273+20; %[K] - absolute temperature



%calculated parameters:

eb=n/(1-n); %[-] - bentonite layer void ratio
Cx=Cx0/eb; %[mol/L] - montmorillonite fixed charge coefficient referred to
the pore space
DCa=D0Ca*tau; %[m^2/s] - calcium effective diffusion coefficient
DNa=D0Na*tau; %[m^2/s] - sodium effective diffusion coefficient
DCl=D0Cl*tau; %[m^2/s] - chlorine effective diffusion coefficient


% differential equations solution:

%FDM PARAMETERS.
nx=41; %[-] - node number
nxx=nx-1;
dx=1/nxx; %[-] - finite distance between two subsequent nodes
x=[0:dx:1]; %[-] - spatial coordinate

tannifin=30/365; %[anni]
t0=L^2/DCa; % [s] - reference time
tfin=tannifin*(60*60*24*365)/t0; % [-] - dimensionless final time
dt=0.0001; % [-] - time discretisation
nt=tfin/dt; % [-] - number of time step
```

```
%INITIAL CONDITIONS.


C0NaCl=0.05; %[mol/L] - initial external sodium chloride concentration
GCl0=-Cx/(2*C0NaCl)+sqrt((Cx/(2*C0NaCl))^2+1);  %[-]  -  chlorine  partition
coefficient
GNa0=GCl0^(-1); %[-] - sodium partition coefficient
CNa0=GNa0*C0NaCl;  %[mol/L]
CCl0=GCl0*C0NaCl;  %[mol/L]


%BOUNDARY CONDITIONS.


alfa=Cx/(2*C0);
aux=(108-(8*(alfa^3))+12*sqrt(81-(12*(alfa^3))))^(1/3);
GCl=real((2/(3*aux))*(alfa^2)-(1/3)*alfa+(1/6)*aux);    %[-]    -    chlorine
partition coefficient
GCa=GCl^(-2); %[-] - calcium partition coefficient
CCl=GCl*C0*2; %[mol/L]
CCa=GCa*C0; %[mol/L]
Cr=CCa; %[mol/L] reference concentration
u1(1)=1;
u2(1)=CCl/Cr;
u1(nx)=1;
u2(nx)=CCl/Cr;


t=0;
for ix=2:nxx
    u1(ix)=0;
    u2(ix)=CCl0/Cr;
end


for ix=1:nx
    u3(ix)=(Cx+CCl0)/Cr;
end
for iw=1:(nx+1)/2
    w1(iw)=u1(iw);
    w2(iw)=u2(iw);
    w3(iw)=u3(iw);
    xw(iw)=x(iw)*2;
end


%CALCULATIONS.


snapt1(1)=u1(nxx/2);
```

```
snapt2(1)=u2(nxx/2);
snapt3(1)=u3(nxx/2);
snaptCx(1)=Cx;
t(1)=0;
snap3D1(1,:)=w1;
snap3D2(1,:)=w2;
snap3D3(1,:)=w3;
tt3D(1)=0;

for it=1:nt
    u1old=u1;
    u2old=u2;
    for ixbis=1:nxx
        u1oldbis(ixbis)=(u1old(ixbis)+u1old(ixbis+1))/2;
        u2oldbis(ixbis)=(u2old(ixbis)+u2old(ixbis+1))/2;

tCa(ixbis)=4*DCa*u1oldbis(ixbis)/(DNa*Cx/Cr+(DNa+DCl)*u2oldbis(ixbis)+(4*DCa-
2*DNa)*u1oldbis(ixbis));

tCl(ixbis)=DCl*u2oldbis(ixbis)/(DNa*Cx/Cr+(DNa+DCl)*u2oldbis(ixbis)+(4*DCa-
2*DNa)*u1oldbis(ixbis));
        D11(ixbis)=-(tCa(ixbis)-tCa(ixbis)*DNa/DCa-1);
        D12(ixbis)=-(tCa(ixbis)/2*DCl/DCa*(DNa/DCl-1));
        D21(ixbis)=-(2*tCl(ixbis)*(DNa/DCa-1));
        D22(ixbis)=-(DCl/DCa*(tCl(ixbis)-tCl(ixbis)*DNa/DCl-1));
    end

    for ix=2:nxx
        d2bu1(ix)=(u1old(ix-1)-u1old(ix))/(dx^2);
        d2bu2(ix)=(u2old(ix-1)-u2old(ix))/(dx^2);
        d2fu1(ix)=(u1old(ix+1)-u1old(ix))/(dx^2);
        d2fu2(ix)=(u2old(ix+1)-u2old(ix))/(dx^2);
        u1(ix)=u1old(ix)+(D11(ix-1)*d2bu1(ix)+D11(ix)*d2fu1(ix)+D12(ix-
1)*d2bu2(ix)+D12(ix)*d2fu2(ix))*dt;
        u2(ix)=u2old(ix)+(D21(ix-1)*d2bu1(ix)+D21(ix)*d2fu1(ix)+D22(ix-
1)*d2bu2(ix)+D22(ix)*d2fu2(ix))*dt;
    end
    for ix=1:nx
        u3(ix)=Cx/Cr+u2(ix)-2*u1(ix);
    end
    t=it*dt;
    snapt1(it+1)=u1(nxx/2);
    snapt2(it+1)=u2(nxx/2);
    snapt3(it+1)=u3(nxx/2);
```

```matlab
        snaptCx(it+1)=Cx;
        for iw=1:(nx+1)/2
            w1(iw)=u1(iw);
            w2(iw)=u2(iw);
            w3(iw)=u3(iw);
        end
        snap3D1(it+1,:)=w1;
        snap3D2(it+1,:)=w2;
        snap3D3(it+1,:)=w3;
        tt(it+1)=t;
        tt3D=[tt3D; t];
end


ttdays=tt*t0/(60*60*24);
tt3Ddays=tt3D*t0/(60*60*24);

%FIGURES.

figure(1);
plot(xw,w1,xw,w2,xw,w3);
legend('C_C_a/C_C_a_0','C_C_l/C_C_a_0','C_N_a/C_C_a_0');
xlabel('X=x/L');ylabel('C/C_C_a_0');
figure(2);
plot(ttdays,snapt1*Cr,ttdays,snapt2*Cr,ttdays,snapt3*Cr,ttdays,snaptCx);
xlabel('Time, t [d]');ylabel('Ion concentration, c_i [mol/L]');
legend('c_C_a','c_C_l','c_N_a','c_s_k');
figure(3);
clf
mesh(xw,tt3Ddays,snap3D1*Cr), grid on
xlabel('Relative distance inside the bentonite layer, x [-]')
ylabel('Time, t [d]')
zlabel('Calcium concentration, c_C_a [mol/L]')
figure(4);
clf
mesh(xw,tt3Ddays,snap3D2*Cr), grid on
xlabel('Relative distance inside the bentonite layer, x [-]')
ylabel('Time, t [d]')
zlabel('Chlorine concentration, c_C_l [mol/L]')
figure(5);
clf
mesh(xw,tt3Ddays,snap3D3*Cr), grid on
xlabel('Relative distance inside the bentonite layer, x [-]')
ylabel('Time, t [d]')
zlabel('Sodium concentration, c_N_a [mol/L]')
```

212

6.5   SIMULATION RESULTS

In this last paragraph the results of the mathematical model, analyzed for CASE A and CASE B, representing the simple and the composite bentonite barrier respectively, are reported. As already described in paragraph 6.1, CASE A consists of a 10 mm Sodium bentonite layer standing between two reservoirs containing the same concentration of Calcium Chloride; while CASE B represents a composite barrier given by a 10 mm Sodium bentonite layer and a Geomembrane posed above. The barrier stands between two reservoirs containing the same concentration of CaCl$_2$ but the GM completely inhibits the diffusive Calcium flux from the upper reservoir to the bentonite layer.

6.5.1. Case A results: 10 mm bentonite layer alone.

The model input data, in terms of bentonite tortuosity, porosity and solid skeleton charge, come from the results of the osmotic and swelling pressure tests performed on sodium bentonite (see chapter 3) and are summarized in Table 6.1.

Table 6.1 – Case A input data.

Description:	Input data:	Unit:
MATERIALS and PORE SOLUTION		
Bentonite layer thickness, L	0.01	m
Bentonite layer porosity, n	0.81	-
Bentonite layer tortuosity coefficient, τ	0.31	-
Montmorillonite electric charge of the solid skeleton, $c_{sk,0}$	0.09	mol/L
Calcium free solution diffusion coefficient, $D_{0,Ca}$	$7.92 \cdot 10^{-10}$	m^2/s
Sodium free solution diffusion coefficient, $D_{0,Na}$	$13.3 \cdot 10^{-10}$	m^2/s
Chlorine free solution diffusion coefficient, $D_{0,Cl}$	$20.3 \cdot 10^{-10}$	m^2/s
Calcium Chloride concentration in the reservoirs, c_0	0.02	mol/L
Initial external Sodium Chloride concentration, $c_{0,NaCl}$	0.05	mol/L
FDM PARAMETERS		
Node number, nx	$31 \div 41$	-
Final time, $t_{yearsfin}$	35/365	Yr
Time discretization, dt	$10^{-4} \div 10^{-5}$	-

With the aim to compute the model solution the following parameter was calculated:

Bentonite layer void ratio, $\qquad e = \dfrac{n}{1-n}$

Montmorillonite fixed charge coefficient referred to the pore space, $\qquad c_{sk} = \dfrac{c_{sk,0}}{e}$

i-th ion effective diffusion coefficient, $\qquad D_i^* = D_{0,i} \cdot \tau$

The obtained results are reported in the following figures: in Figure 6.10 Calcium, Chlorine and Sodium concentration trends in time are plotted in correspondence of the bentonite layer median node; in Figures 6.11 Calcium, Chlorine and Sodium relative concentrations are plotted as a function of the relative distance inside the bentonite layer in four selected simulation moments (15 minutes, 2.5 hours, 12 hours, 1 day). Moreover, in Fig. 6.12, 6.13 and 6.14 Calcium, Chlorine and Sodium concentrations are plotted as a function of both the time and the relative distance inside the bentonite layer.

Figure 6.10 – Calcium, Chlorine and Sodium concentration trends as a function of time.

Figure 6.11 – Relative ion concentration as a function of the relative distance inside the layer at 15 minutes (dash-dotted line), 2.5 hours (dotted line), 12 hours (dashed line) and 1 day of simulation (continuous line).
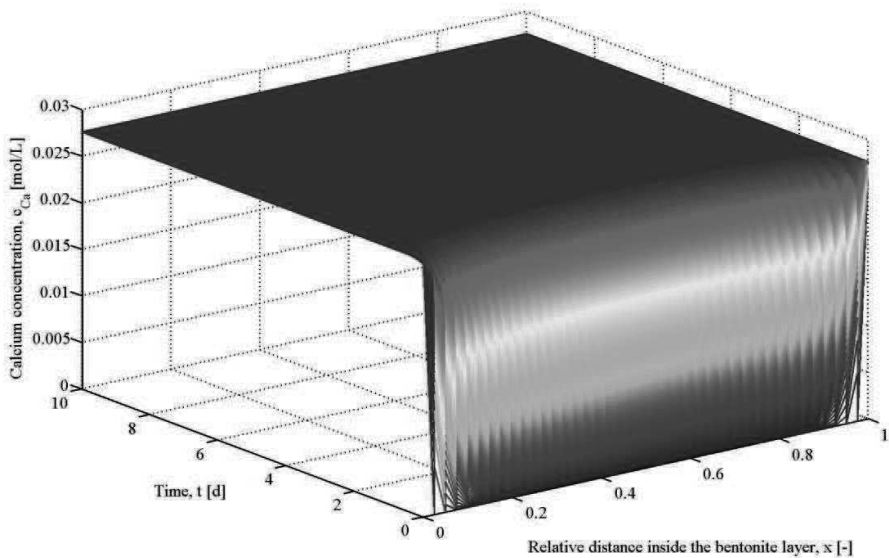

Figure 6.12 – Calcium concentration as a function of both time and relative distance inside the layer.
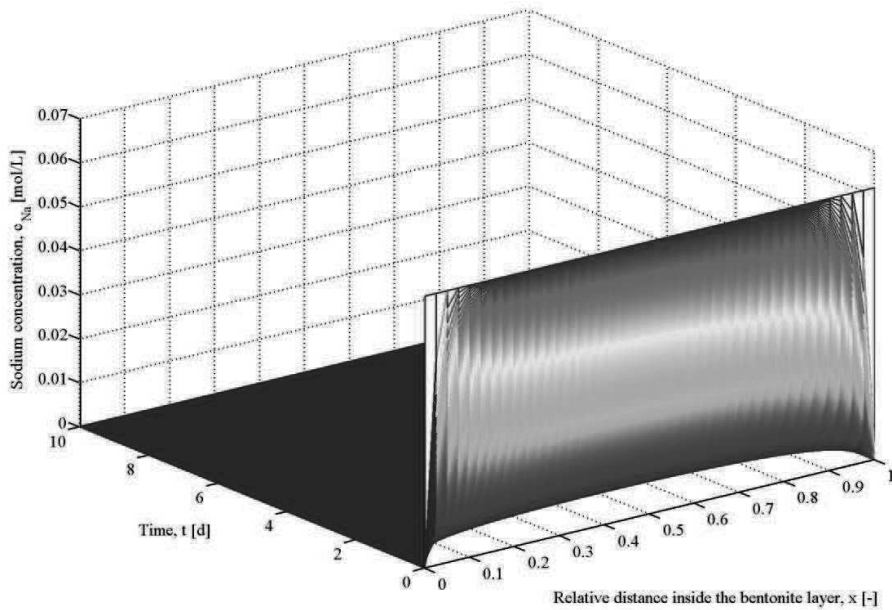
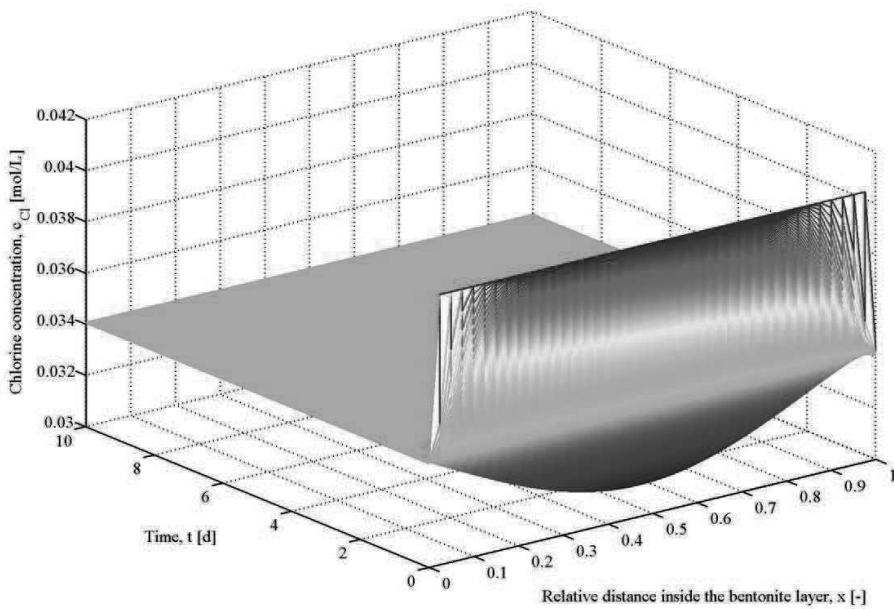Figure 6.13 – Sodium concentration as a function of both time and relative distance inside the layer.

Figure 6.14 – Chlorine concentration as a function of both time and relative distance inside the layer.

216

6.5.2 Case B results: composite barrier.

The results, that will be reported for CASE B, was obtained using the MATLAB$^{®}$ script listed in the previous paragraph.

The 'no flux' boundary condition, next to the GM, is simulated by constructing a virtual and mirror bentonite layer over the GM limit. In this way, to the position of the GM in the 'true' model corresponds the median node of the 'virtual and mirror' model. In this particular node the flux is null due to the 'virtual and mirror' model symmetry.

The input data for CASE B are equal to those listed for case A, except for the bentonite layer thickness that is doubled, as explained above, for the model requirements.

The obtained results are reported in the following figures: in Figure 6.15 Calcium, Chlorine and Sodium concentration trends in time are plotted in correspondence of the ('true') bentonite layer median node; in Figures 6.16 Calcium, Chlorine and Sodium relative concentrations are plotted as a function of the relative distance inside the bentonite layer in four selected simulation moments (15 minutes, 2.5 hours, 12 hours, 1 day). The relative distance inside the bentonite layer results, in this case, equal to 0 next to the lower boundary, while it is equal to 1 next to the GM.

Moreover, in Fig. 6.17, 6.18 and 6.19 Calcium, Chlorine and Sodium concentrations are plotted as a function of both the time and the relative distance inside the bentonite layer (which is equal to 0 next to the lower boundary, while it is equal to 1 next to the GM).
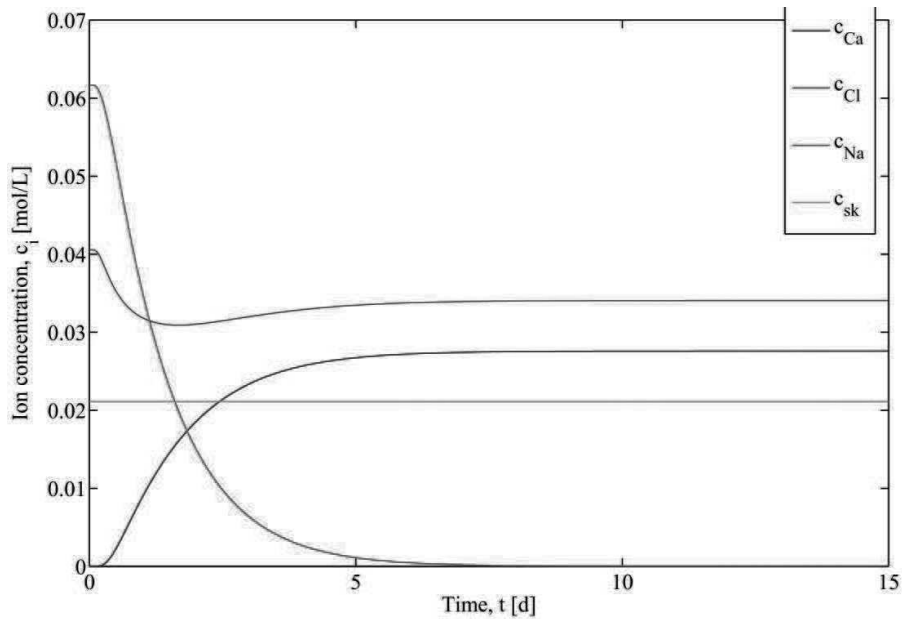
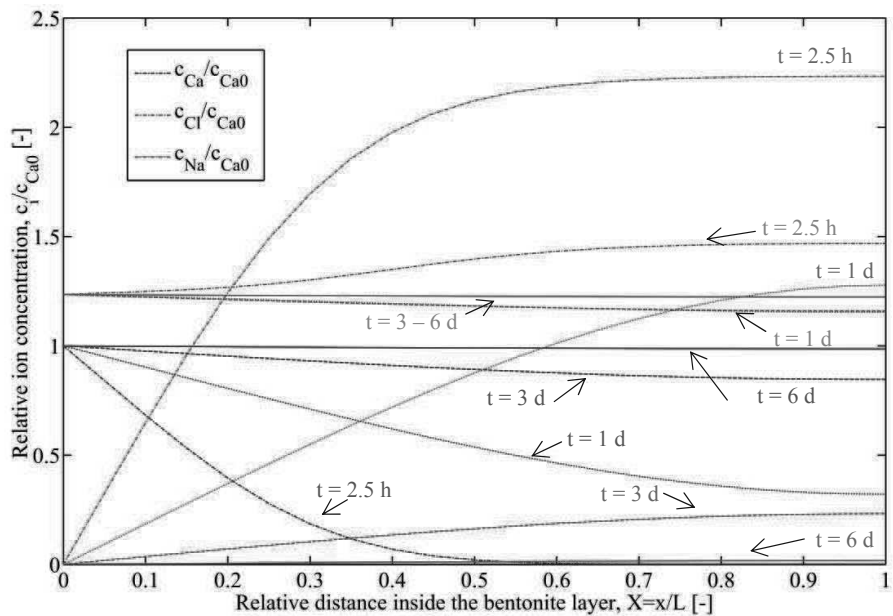Figure 6.15 – Calcium, Chlorine and Sodium concentration trends as a function of time.

Figure 6.16 – Relative ion concentration as a function of the relative distance (0 next to the lower boundary, 1 next to the GM) inside the layer at 2.5 hours (dash-dotted line), 1 day (dotted line), 3 days (dashed line) and 6 days of simulation (continuous line).
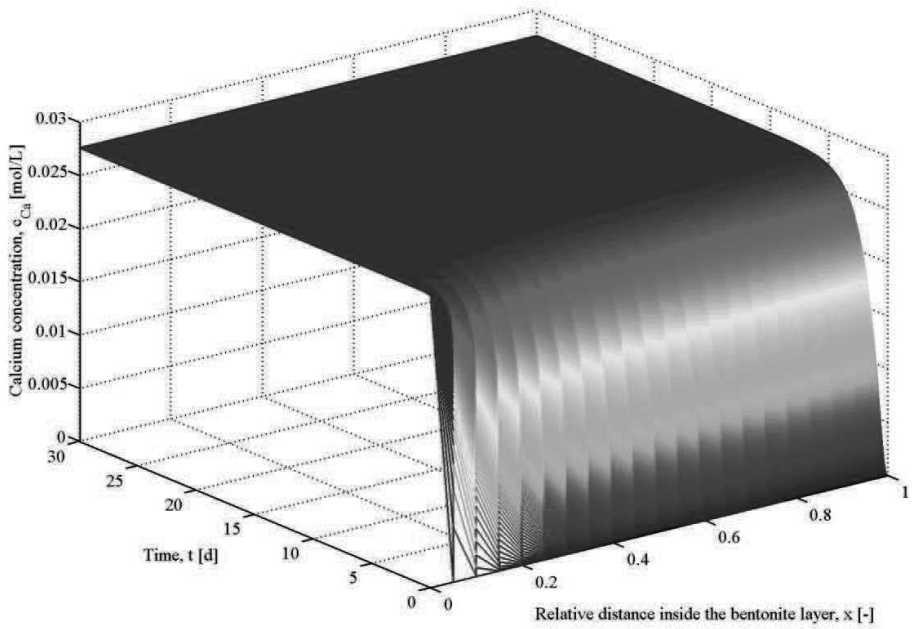
Figure 6.17 – Calcium concentration as a function of both time and relative distance inside the layer.
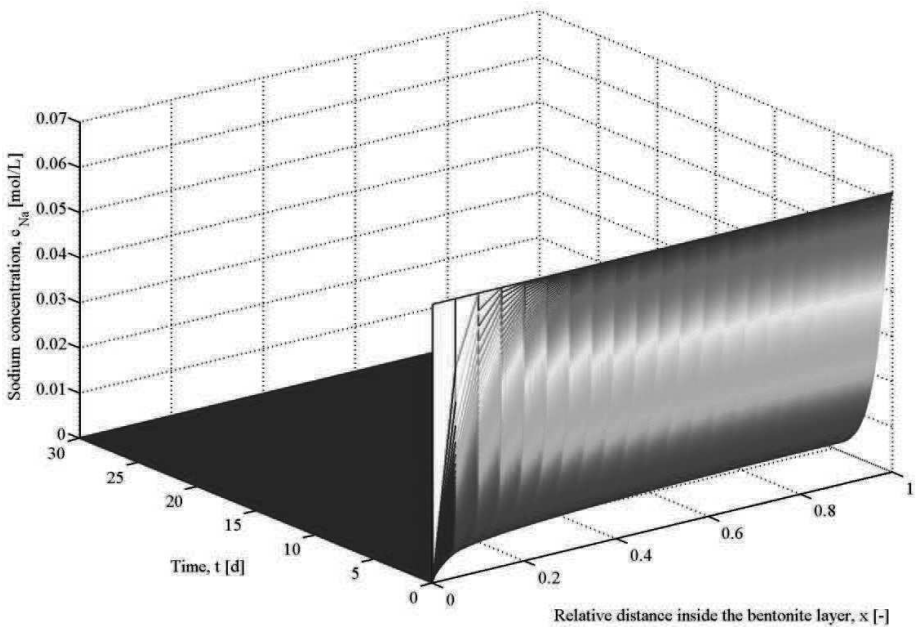

Figure 6.18 – Sodium concentration as a function of both time and relative distance inside the layer.
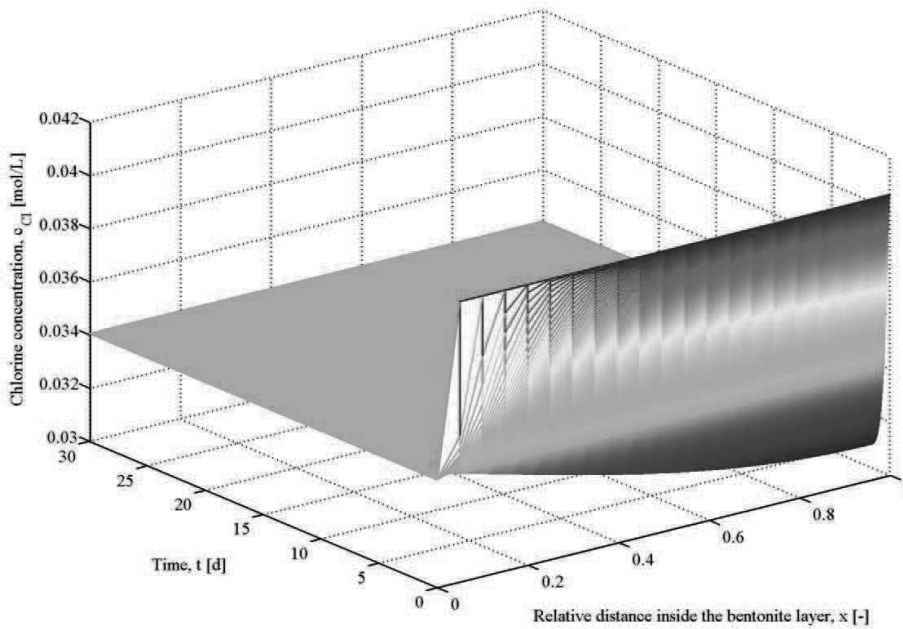
Figure 6.19 – Chlorine concentration as a function of both time and relative distance inside the layer.

6.5.3 Confront with literature experimental data

Shackelford and Lee (2003) reported the results of a combined chemico-osmotic/diffusion test conducted on a GCL containing sodium bentonite using a 5 mM $CaCl_2$ solution. In the test a time-dependent membrane efficiency was derived from the test, performed as described in paragraph 3.5.2.1 for the chemico-osmotic tests carried out for the Ph.D. experimental programme.

The results obtained by Shackelford and Lee (2003) are reported in Fig. 6.20 in term of chemico-osmotic efficiency (i.e. global reflection coefficient) as a function of time; Fig 6.21 in term of cumulative calcium mass per unit are as a function of time.
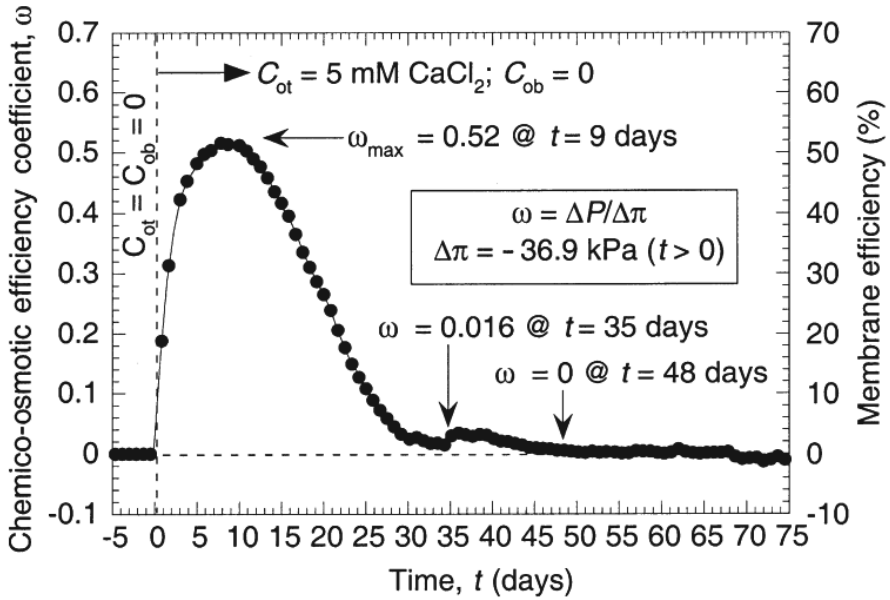
Figure 6.20 – Calculated chemico-osmotic efficiency (i.e. global reflection coefficient) as a function of time (after Shackelford and Lee, 2003).
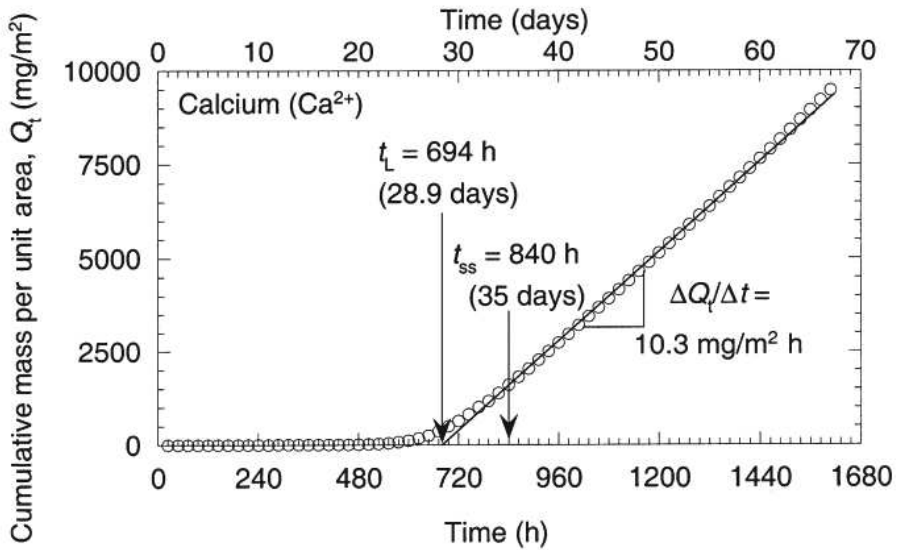

Figure 6.21 – Cumulative mass data based on measured bottom concentrations (t_L = time lag; t_{SS} = time to steady-state diffusion) (after Shackelford and Lee, 2003).

In Fig. 6.20 an initial increase of the global reflection coefficient is observed to a peak value of 0.52, which corresponded to the characteristic value for the sodium bentonite GCL at the test conditions (mineralogy of the used bentonite, concentration gradient and state variable, i.e. porosity). The peak was followed by a gradual decrease to zero induced by the cation exchange of calcium for sodium and the consequent aggregation of lamellae in tactoids at microscopic scale.

The zero value of the reflection coefficient, reached after 35 days of test, is consistent with the data obtained for the calcium bentonite with the 5 mM $CaCl_2$ solution in the test performed during the development of the Ph.D. experimental activity (see paragraph 3.9.1).

At the end of the test reported by Shackelford and Lee (2003), the semipermeable behaviour initially observed on sodium bentonite was completely destroied and the specimen behaved as a calcium bentonite specimen.

Moreover, the time required to achieve the steady state calcium diffusion through the specimen (i.e. $t_{SS} = 35$ days, in Fig. 6.21) correlated well with the time required for having the zero value of global reflection coefficient.

This result proved the correlation between the achievement of the complete saturation of the exchange centres with calcium (after that calcium diffusion through the specimen was no more delayed) and the complete transition from a behaviour typical of sodium bentonite (membrane behaviour presence) to a behaviour typical of calcium bentonite.

Althounghth the boundary conditions in chemico-osmotic test correspond to perfect flushing conditions, which are very difficult to simulate in a matematical model, the results reported by Shackelford and Lee (2003) can be roughly compared with the simulation results obtained for Case B.

A no flux boundary exists in the model in corrispondence to the GM which does not correctly rapresents the perfect flushing boundary condition of the top porous stone, saturated with DW. The analogy between the test and the Case B conditions is that in both cases there is not calcium flux from the upper boundary, but only from the lower reservoir, where the calcium concentration is mantained constant.

The comparison shows that the model tends to understimate the time necessary to achieve the chemical equilibrium (i.e. to completely transform the sodium bentonite

specimen in calcium bentonite), which is lower than 10 days in the model and higher than 30 days in the test.

In the proposed model the pore space consists of a single volume of interparticle pores where the transport of the cationic species is assumed to occur through diffusion. Sorption sites are assumed to exist on the surface of solid particles and instantaneous exchange of cations is assumed to occur between the mineral surface and the pore solution.

This representation is indeed an approximation of reality. A more realistic model should represent the pore space as a three-component structure consisting of three separated compartments: the intergranular pores, the interparticle pores and interlayer pores. Diffusive flux occurs from the intergranular to the interparticle pores and from the interparticle pores to the interlayer pores, as schematically represented in Fig. 6.22 (Jo et al., 2006).
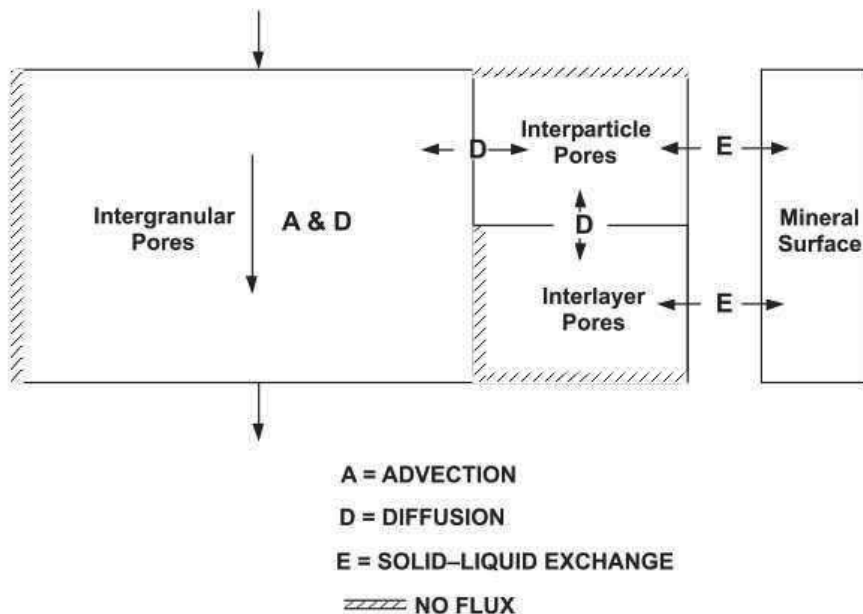

Figure 6.22 – Schematic representation of the three-compartment pore space (after Jo et al. 2005).

Sorption sites are assumed to exist on the surfaces in both the interparticle and interlayer pores and simultaneous exchange occurs between the mineral surface and these two pores compartments.

Since the cations need to diffuse through the three compartments to reach all the sorption sites, the steady state is reached when the concentration equilibrium conditions are achieved in all the compartments.

While the proposed model assumes a instantaneous concentration equilibrium in the pore volume, a finite transition time is necessary to achieve concentration equilibrium between the three compartments. Therefore, the rate of the cation exchange phenomenon could be overestimated in the model since the transition phase is neglected.

6.5.4 Result discussion

The results obtained in this study highlight the importance of the Calcium diffusion contribution to the development of the cation exchange phenomenon in a GCL.

As underlined by Shackelford (2005), in laboratory conditions, characterized by high hydraulic gradient, the role of Calcium advective contribution is predominant and, as a consequence, the time necessary to reach chemical equilibrium is strongly influenced by the applied hydraulic gradient.

Otherwise, in field conditions, where the hydraulic gradient is lower (e.g. $i \approx 30$), and especially when low permeability material (i.e. Sodium bentonite) are considered, the volumetric water flux across the bentonite layer may decrease so much to result unimportant if compared with the contribution of the diffusive flux induced by the Calcium concentration gradient existing from outside to inside the GCL.

Moreover, this study demonstrates that the development in time of the cation exchange phenomenon, as a consequence of the diffusive Calcium flux, is much faster than those values individuated by Shackelford (2005), for field conditions, taking into account the only advective Calcium flux (i.e. tens of years).

With the aim to facilitate the comparison with the other data, in this study, the Calcium Chlorine concentration insisting on the GCL was assumed equal to that individuated by Shackelford (2005). It is important to underline that a 20 mM

solution represents an average and representative Calcium concentration for the leachate and the common soil pore solution.

The results obtained for CASE A (10 mm Sodium bentonite layer standing between two reservoirs containing the same concentration of Calcium Chloride) and for CASE B (composite barrier given by a 10 mm Sodium bentonite layer and a Geomembrane posed above) show that the time necessary to achieve the chemical equilibrium is lower than 10 days in both barrier configurations.

The comparison with the experimental results obtained by Shackelford and Lee (2003), highlight that the model tends to overestimated the velocity of the cation exchange phenomenon because of the approximation deriving from the representation of the pore space as a single volume characterized by an average tortuosity value. This approximation generates an overestimation of the diffusion rate in the smaller and more tortuous pores (i.e. interlayer pore space).

In any case, the results obtained with the mathematical model can be compared with the experimental data (Shackelford and Lee, 2003). In both cases the cation exchange phenomenon ends in some tens of days.

In field conditions, where the saturation of the bentonite layer is inconstant in time, the cation exchange phenomenon development can slow down but the chemical equilibrium is reached in a time anyway lower than one year.

Since the time required satisfy the typical long term landfill requirements is 50-70 years, the results obtained underline the importance to develop innovative products able to maintain good hydraulic performance even in presence of multivalent electrolyte solutions.

REFERENCES

Bellomo N. and Preziosi L. (1995). Modelling mathematical methods and scientific computation. Boca Raton. CRC.

Dominijanni A. (2005). Osmotic properties of clay soils. PhD thesis. Politecnico di Torino.

Jo, H. Y., Benson, C. H., Edil, T.B. (2006). Rate-limited cation exchange in thin bentonitic barrier layers. Canadian Geotechnical Journal, **43**, 370-391.

Shackelford, C.D. (2005). Environmental issues in geotechnical engineering. In Proceedings of the 16th International Conference on Soil Mechanics and Geotechnical Engineering, vol. 1, September 12-16, 2005, Osaka, Japan. Millpress Science Publishers, Rotterdam, The Netherlands, pp. 95-122.

Shackelford, C. D. and Lee, J. M. (2003). The destructive role of diffusion on clay membrane behaviour. Clays and Clay Minerals, **5**(2), 186-196.

FINAL CONCLUSIONS

The aim of the Ph.D. research work is to analyse possible improvements of bentonite barriers, in order to enhance the containment performances of the bentonitic component towards non standard permeants, such as electrolyte solution and hydrocarbons.

The study described in this Ph.D. thesis has been supported by an ample laboratory activity, which has been developed at the laboratory of soil mechanics of the Department of Environment, Land and Infrastructure Engineering and at the Disaster Planning Laboratory of the Department of Structural, Geotechnical and Building Engineering of the Politecnico di Torino, with an exception for the swell pressure tests, which have been performed at ISMGEO (Seriate, Milan, Italy).

The phenomenological and physical description of the mineralogical, chemical and physical properties of bentonite is reported in some detail in the first chapter.

The excellent swelling and hydraulic properties of sodium bentonite are exposed together with the disadvantage represented by the potential for cation exchange of Sodium with Calcium (dominant in the pore water of many soils), which tends to neutralize the charges within the tactoids and, consequently, to increase tactoid size, with the associate reduction in swelling, reduction in specific surface of the material and consequent increase in permeability.

The first chapter affects furthermore an experimental study on the difference in the swelling and mechanical behaviour of sodium and calcium bentonite.

At the microscopic scale, a dispersed structure of separated lamellae, can be attributed to sodium bentonite, while an aggregated structure formed by packets of

lamellae united in a parallel face-to-face array (i.e. tactoids) can be attributed to calcium bentonite. The results of the liquid limit and swell index determinations, swelling tests and loading/unloading tests, performed on sodium and calcium bentonite, highlighted that the microscopic scale structure has a deep influence on the swelling and mechanical properties of bentonite. In particular, the tests performed on calcium bentonite showed a significant inhibition of the swelling behaviour typical of sodium bentonite, even with de-ionized water and very low molarity electrolyte solution.

The evidence of the strong degradation induced in the swelling performances of bentonite by the cation exchange phenomenon highlights the need to develop innovative materials or innovative techniques aimed at improving the resistance of the bentonite barriers to the degradation induced by the cation exchange phenomenon, in order to comply with the legislation requirements on landfill barrier performances and the maintenance of these performances in time.

About this last issue, the role of physical pretreatments on natural and polymer modified bentonites and the effect of the presence or absence of needling across the bentonite layer have been analysed in the laboratory simulation of both short and long term landfill conditions (i.e. before and after the cation exchange completion).

The results of this study, reported in chapter 2, showed that physical pretreatments strongly influence the swelling and hydraulic behaviour of bentonite specimens exposed to calcium solutions and that the presence of needling deteriorates the hydraulic performances of specimens to a great extent in long term conditions.

In particular, the pre-hydrated and pre-consolidated specimens showed no hydraulic conductivity value variation after cation exchange phenomenon completion. This is a very important result that is in contrast with the trend generally registered for loose specimens and that suggests the pre-consolidation treatment as the favourite for the hydraulic performance maintenance in long term.

Moreover, the results obtained with the specimen subjected to salt removal and pre-consolidation showed higher hydraulic performance with both deionized water and $CaCl_2$ solution, as a consequence of the reduction in the initial cation concentration in the pore solution which leads to an initial more dispersed and homogeneous configuration at the microscopic scale.

The tests performed on polymer modified specimens showed hydraulic conductivity values to deionized water that were approximately one order of magnitude lower than those obtained for natural specimens, highlighting an excellent result with regard to the use of the polymer Nanosponge. Unfortunately, during the permeation with water and the Calcium solution, the polymer was solubilised and the results of the spectroscopy substantially showed the absence of the polymer in the specimens at the end of the tests.

In chapter 3 the semi-permeable membrane behaviour of bentonite, induced by the electric interaction between the montmorillonite solid skeleton and the ions contained in the pore solution, is analysed under the theoretical and experimental viewpoint. The chemico-osmotic and swelling properties of powder bentonites were studied through a systematic laboratory activity including chemico-osmotic tests and swell pressure tests.

An original salt removal method was developed, called *squeezing*, with the aim to reduce the salt removal time by subjecting the natural bentonite to a series of consecutive phases of powder bentonite hydration with deionized water and drained consolidation, performed in a consolidometer. The proposed method can produce about 500 g of "salt-less" dry powder bentonite in 40-50 days, reducing the salt removal time of the common *flushing* method, which requires many months or even a year to obtain the same results.

The experimental activity consisted of a chemico-osmotic test and a series of swelling pressure tests, performed on the same squeezed bentonite characterized by a porosity value equal to n = 0.81 with the same series of electrolyte concentrations (5, 10, 20, 50 and 100 mM NaCl), aimed at compare the osmotic and swelling behaviour of sodium bentonite. The results of these tests, reported in the paper in chapter 3, highlighted that the global reflection coefficient, which measures the osmotic efficiency of the material, and the swelling pressure tend to decrease as the NaCl concentration increases. In particular, the global reflection coefficient has resulted to range from 68% for 5 mM NaCl concentration to 5% for 100 mM NaCl concentration and was assumed null for higher molarities, while the swelling pressure ranged from 25 kPa for 5 mM NaCl concentration to 0 kPa for 100 mM NaCl concentration. The results of the tests have been used to derive the electric

charge of the solid skeleton, $\overline{c}_{sk,0}$, using the model derived by Dominijanni (2005) and proposed in the first part of the co-authored paper. For both the chemico-osmotic test results and the swelling pressure results, the best fitting of the theoretical curves with the experimental data, a value of $\overline{c}_{sk,0}$ equal to 90 mM was found, highlighting an excellent model consistency.

The chemico-osmotic properties of calcium bentonite, evaluated using the same procedure adopted for sodium bentonite, resulted very low and ranged from 0.5%, for a 5 mM $CaCl_2$ concentration, to 0.2%, for a 10 mM $CaCl_2$ concentration.

Starting from the knowledge achieved during the laboratory activity on both the osmotic and the swelling pressure tests, a new apparatus was designed, aimed at measuring together the global reflection coefficient, ω_g, the global effective diffusion coefficient, $D^*_{\omega g}$, and the swelling pressure, u_{sw}, of bentonites, and it is still underway in the laboratory of ISMGEO.

The results obtained in chapter 2 and 3, concerning the strong degradation induced by the cation exchange phenomenon on hydraulic, swelling and osmotic performance of sodium bentonite, have underlined the need to study the temporal development of the cation exchange phenomenon with the aim to compare that to the period in which landfill barrier performances have to be guaranteed in in-situ conditions. In particular, the mathematical study developed in chapter 6 is focused on the evaluation of the role of the diffusive component of Calcium flux in the cation exchange phenomenon in-situ conditions.

A mathematical model was developed, which describe a simplified scheme consisting of a "three ions + water solvent + charged solid" system taking into account the osmotic behaviour, with two dimensionless equations (describing the simplified system in time and in space) that constituted a non-linear parabolic system. The dimensionless equation system was discretized using finite differences centred in space and the forward Euler method in time and then implemented in MATLAB[®].

The simulation results showed that the development in time of the cation exchange phenomenon, as a consequence of the diffusive Calcium flux, is lower than 10 days and is much faster than those values that can be individuated taking into account the

only advective Calcium flux (i.e. tens of years). Moreover, even if the comparison with literature experimental results outlines that the model tends to overestimate the velocity of the cation exchange phenomenon, the results obtained with the mathematical model can be compared with the experimental data (Shackelford and Lee, 2003). In both cases the cation exchange phenomenon ends in some tens of days.

Since the time required satisfy the typical long term landfill requirements is 50-70 years, the results obtained underline the importance to develop innovative products able to maintain good hydraulic performance even in presence of multivalent electrolyte solutions.

The chemical compatibility of sodium bentonite with calcium solution is only one of the issues concerning the long term performance of the material. The permeation of bentonite with organic compounds, characterized by very low value of dielectric constant, induces the aggregation of bentonite lameallae at the microscopic scale as well as the cation exchange phenomenon. Since in the last decade, new geosynthetic clay liner applications, requiring their use for hydrocarbon secondary containment to prevent subsoil dispersion of accidental oil spills through primary lining system (generally HDPE) from hydrocarbon storage tanks, have found growing interest, an experimental study was developed aimed at evaluating possible materials or techniques aimed at increase the hydrocarbon containment performances of bentonite. The results of the study, reported in chapter 4, show that the hydraulic performances of the partially pre-hydrated geosynthetic clay liner tested with diesel oil decreases as the initial water saturation decreases. In particular, when the initial water content of the geosynthetic clay liner is lower than 100%, the permeation with diesel oil induces the formation of cracks and macropores, that behave as preferential pathways for hydraulic flow and determine very high value of hydraulic conductivity to diesel oil.

Moreover, the permeability of the polymer modified specimen to diesel oil resulted one order of magnitude lower than the value measured testing the dry GCL.

Finally, during the development of the PhD, the possibility to use bentonite in bentonite-based barriers containing incinerator bottom ashes was evaluated for landfill capping purposes. The results of this study, reported in chapter 5, showed

that incinerator bottom ashes are made up of heterogeneous sand-like materials that present several physical and mechanical advantages, compared to natural filling materials, but are not characterized by a hydraulic conductivity sufficiently low to satisfy Italian standard requirements for landfill cover hydraulic barriers. The bottom ash-bentonite mixture (at 10% bentonite content by weight) showed a steady-state hydraulic conductivity of $8 \cdot 10^{-10}$ m/s which was more than one order of magnitude lower than that required by Italian legislation concerning landfill covers. Moreover, as far as heavy metal release is concerned, the column leaching test suggested a positive effect, due to the heavy metal absorption on bentonite, which decreased the potential release of contaminants from bottom ash, but did not inhibit the bentonite swelling behaviour.

FINAL ACKNOWLEDGMENTS

Giunta la fine di un percorso durato così a lungo, desidero utilizzare quest'ultima pagina per ringraziare tutte le persone che hanno collaborato per la realizzazione di questo lavoro di ricerca.

Il Professor Mario Manassero e Andrea Dominijanni per il loro entusiasmo, la loro guida e il loro costante ed indispensabile aiuto nello sviluppo di questo progetto di ricerca.

I tesisti, che sono stati fondamentali nella realizzazione di una così ampia attività di laboratorio: Michela Cravero, Silvia Manzone, Valentina Ferraris, Christian Arneodo, Andrea Sburlati, Marta Tuninetti, Silvia Calò, Irene Gambino, Cristina Vidali e Giacomo Boffa.

Roberto Maniscalco, che è stato colonna portante della predisposizione delle nostre attrezzature di laboratorio, al quale devo tantissimi consigli e tantissime nozioni tecniche.

Giampiero Bianchi, che ci ha aiutato così tante volte, anche quando la situazione in laboratorio sembrava disperata (e non lo era).

Il Prof. Francesco Trotta e Marco Zanetti della Facoltà di Chimica Organica dell'Università degli Studi di Torino, che hanno collaborato con noi nella preparazione delle bentoniti modificate con polimeri.

Il Prof. Vincenzo Fioravante, Andrea Saccenti e Giuseppe Angeloni, di ISMGEO, che hanno collaborato con noi nella realizzazione di una parte dell'attività sperimentale.

Il Prof. Franco Marchese, che ha realizzato le analisi chimiche sulla miscela scorie-bentonite ed è co-autore dell'articolo su Waste Management & Research.

Tutti i miei colleghi e compagni di viaggio in questi anni di Dottorato presso il Politecnico di Torino, in particolare, Manuela Alferi, Carmine Terriori e Luca Buffa.

Infine, il più grande ringraziamento va ai miei genitori e a Stefano, perché la loro fiducia e il loro supporto sono quotidiani ed incondizionati, e mi rendono una persona migliore.